Free-Space Microwave Imaging through Alphabet-Based Bayesian Compressive Sensing

N. Alselmi, G. Oliveri, M. A. Hannan, M. Salucci, and A. Massa

Abstract

A key requirement to be satisfied when exploiting Compressive Sensing (*CS*) methods in inverse scattering (*IS*) problems is that the unknowns (e.g., the contrast function or the equivalent sources) are *sparse* with respect to the considered expansion basis. State-of-the-art *CS*-based microwave imaging techniques typically consider single-resolution pixel-based representations, limiting their domain of applicability to the retrieval of few and isolated pixels within the investigated domain. Within this framework, this work is aimed at extending the range of applicability of *CS*-based approaches to the retrieval of unknown scatterers having arbitrary shape and dimensions. Since in real applications no *a-priori* information about the investigation domain is available, the idea is to retrieve a set of "candidate" solutions by executing several *CS* inversions using different expansion bases (e.g., pixel, Haar wavelets, Meyer wavelets, ...). Following the *CS* paradigm, the "best" solution can then be identified as the sparsest one, i.e., the solution with the lowest number of non-zero retrieved coefficients. A preliminary numerical validation of the proposed alphabet-based *CS* microwave imaging technique is given. Some numerical comparisons with competitive state-of-the-art inverse scattering techniques is shown, as well.

1 Mathematical Formulation

Let us consider a homogeneous lossless non-magnetic two-dimensional ($2D$) investigation domain D_{inv} with permittivity ε_0 containing an unknown dielectric target described by the contrast function

$$\tau(\mathbf{r}) = [\varepsilon_r(\mathbf{r}) - 1] - j\left[\frac{\sigma(\mathbf{r})}{2\pi f \varepsilon_0}\right] \tag{1}$$

where $\varepsilon_r(\mathbf{r})$ and $\sigma(\mathbf{r})$ denote the relative permittivity and conductivity at position $\mathbf{r} = (x, y)$, respectively. By denoting with $\xi^v_{inc}(\mathbf{r})$ the v-th known incident transverse-magnetic (TM_z) field impinging on the unknown object ($v = 1, ..., V$), the scatted field can be computed as

$$\xi^v_{scatt}(\mathbf{r}) = \xi^v_{tot}(\mathbf{r}) - \xi^v_{inc}(\mathbf{r}) \tag{2}$$

where $\xi^v_{tot}(\mathbf{r})$ is the total field measured at position $\mathbf{r}$ in the presence of the object. By assuming a time-harmonic condition [the time dependency factor $exp(-j2\pi ft)$ being omitted hereinafter] under the first-order Born approximation ($BA - I$) the following Lippman-Schwinger integral equation models the relationships between the scattered field and the contrast function

$$\begin{gathered}\xi^v_{scatt}(\mathbf{r}) = \int_{D_{inv}} \tau(\mathbf{r}')\, \xi^v_{inc}(\mathbf{r}')\, \mathcal{G}(\mathbf{r}/\mathbf{r}')\, d\mathbf{r}' \\ \mathbf{r} \in D_{obs},\ \mathbf{r} \notin D_{inv},\ v = 1, ..., V\end{gathered} \tag{3}$$

where D_{obs} is the so-called observation domain, external to D_{inv}, and $\mathcal{G}(\mathbf{r}/\mathbf{r}')$ is the two-dimensional free-space Green's function. In order to retrieve the unknown contrast function by solving Eq. (3), we consider the expansion of the problem unknowns with respect to a given basis $\mathbf{B}_f$ made of N basis functions

$$\mathbf{B}_f = \{\psi_{f,1}(\mathbf{r}), ..., \psi_{f,N}(\mathbf{r})\} \tag{4}$$

as follows

$$\tau_f(\mathbf{r}) = \sum_{n=1}^{N} c_{f,n} \psi_{f,n}(\mathbf{r}). \tag{5}$$

In Eq. (5) $c_{f,n}$, $n = 1, ..., N$ are the entries of the coefficient vector $\mathbf{c}_f$ that represents the function $\tau_f(\mathbf{r})$ in the representation domain defined by the basis $\mathbf{B}_f$. By substituting Eq. (5) in Eq. (3), the following discretized version of the integral equation can be easily obtained

$$\begin{gathered}\xi^v_{scatt}(\mathbf{r}) = \sum_{n=1}^{N} c_{f,n} \times \left[\int_{D_{inv}} \psi_{f,n}(\mathbf{r}')\, \xi^v_{inc}(\mathbf{r}')\, \mathcal{G}(\mathbf{r}/\mathbf{r}')\, d\mathbf{r}'\right] \\ \mathbf{r} \in D_{obs},\ \mathbf{r} \notin D_{inv},\ v = 1, ..., V.\end{gathered} \tag{6}$$

If we consider that the scattered field is collected at M measurement points located in $\mathbf{r}_m^v \in D_{obs}$ $(m = 1, ..., M)$ the following system of linear equations is obtained

$$\widetilde{\xi}_{scatt}^v(\mathbf{r}_m^v) = \sum_{n=1}^N c_{f,n} \times \left[\int_{D_{inv}} \psi_{f,n}(\mathbf{r}') \, \xi_{inc}^v(\mathbf{r}') \, \mathcal{G}(\mathbf{r}_m^v / \mathbf{r}') \, d\mathbf{r}'\right] + n^v(\mathbf{r}_m^v) \quad m = 1, ..., M, \; v = 1, ..., V \tag{7}$$

where $n^v(\mathbf{r}_m^v)$ is a sample of an additive white Gaussian noise ($AWGN$) with unknown variance η_v^2. Finally, Eq. (7) can be rewritten in matrix form as follows

$$\widetilde{\boldsymbol{\xi}}_{scatt}^v = \boldsymbol{\Psi}^v \mathbf{c}_f + \mathbf{n}^v \tag{8}$$

where $\widetilde{\boldsymbol{\xi}}_{scatt}^v = \left\{\widetilde{\xi}_{scatt}^v(\mathbf{r}_m^v), \; m = 1, ..., M\right\}$, $v = 1, ..., V$ is the scattered field vector, $\mathbf{n}^v = \{n^v(\mathbf{r}_m^v), \; m = 1, ..., M\}$, $v = 1, ..., V$ is the noise vector, and

$$\boldsymbol{\Psi}^v = \left\{\left[\int_{D_{inv}} \psi_{f,n}(\mathbf{r}') \, \xi_{inc}^v(\mathbf{r}') \, \mathcal{G}(\mathbf{r}_m^v / \mathbf{r}') \, d\mathbf{r}'\right], \; m = 1, ..., M, \; n = 1, ..., N\right\} \tag{9}$$

is the kernel matrix. When the unknown vector $\mathbf{c}_f$ contains few non-null entries, Eq. (8) becomes representative of a sparse problem. In this case, the inverse problem at hand can be successfully solved by means of CS-based inversion techniques, without the need of any assumption on the scatterer shape and dimensions. In the following, a Bayesian version of the standard CS (BCS) is used in order to retrieve an estimate $\widehat{\mathbf{c}}_f$ of the the unknown vector $\mathbf{c}_f$. More in details, $\widehat{\mathbf{c}}_f$ is computed as

$$\widehat{\mathbf{c}}_f = \frac{1}{V} \sum_{v=1}^V arg\left\{\max_{\mathbf{c}_f}\left[\mathcal{P}\left(\mathbf{c}_f \left| \widetilde{\boldsymbol{\xi}}_{scatt}^v \right.\right)\right]\right\} \tag{10}$$

where $\mathcal{P}\left(\mathbf{c}_f \left| \widetilde{\boldsymbol{\xi}}_{scatt}^v \right.\right)$ denotes the posterior density function of $\mathbf{c}_f$ given $\widetilde{\boldsymbol{\xi}}_{scatt}^v$ and is computed by means of the multi-task (MT) version of the BCS method ($MTBCS$). Such a version, unlike the single-task BCS ($STBCS$) also takes into account the correlation between the scattered data collected under different views.

1.1 Proposed Methodology

Since the concept of sparsity of the solution strongly depends on the selected representation basis $\mathbf{B}_f$, the proposed method makes use of an alphabet of F different bases

$$\mathbf{A} = \{\mathbf{B}_1, \mathbf{B}_2, ..., \mathbf{B}_f, ..., \mathbf{B}_F\}. \tag{11}$$

For each considered basis ($f = 1, ..., F$), the $MTBCS$ approach is used to solve the linear system of equations in Eq. (8) in order to retrieve F estimations of the vector of unknowns (i.e., $\{\widehat{\mathbf{c}}_f, \; f = 1, ..., F\}$). Finally, the sparsest solution can be selected by counting the number of non-zero entries (NNZ) of each retrieved vector

$$\gamma_f = NNZ(\widehat{\mathbf{c}}_f) \tag{12}$$

and the "best" solution is then selected as the sparsest one

$$\widehat{\mathbf{c}}_{best} = arg \min_{f=1,...,F} \{\gamma_f\}. \tag{13}$$

1.2 Thresholding

When the inversion is performed using noisy data, the sparsity measure γ_f is unavoidably corrupted by unwanted non-zero coefficients. These unwanted coefficients are not useful for a true scatterer representation, therefore their presence are not desired for the voting criterion. As a consequence we should some how detect these unwanted coefficients in order to be not considered in the sparsity measure γ_f. A straight approach is to use a threshold in NNZ and eliminate during the counting, the coefficients that are under the threshold.

- **Energy based Threshold**

  In order to choose a threshold, independently by the noise level, corrupting the measured data, the threshold is computed as a function of the retrieved coefficient energy $E(\widehat{\mathbf{c}}_f)$, computed as

  $$E\left(\widehat{\mathbf{c}}_f\right) = \sum_{n=1}^{N} |c_{f,n}|^2 \tag{14}$$

  Then the threshold T is computed as a percentage of E, i.e

  $$T = pE \tag{15}$$

  with $0 < p < 1$ defining the percentage of total energy. The subset of coefficients having a total energy which is less than the threshold T are then set to zero.

1.3 Voting and Thresholding

- **Non-Zero Counting Function** $NNZ\left(\mathbf{x}\right)$:

  The function $NNZ\left(\mathbf{x}\right)$ counts the number of non-zero coefficients of the vector $\mathbf{x}$:

  $$NNZ\left(\mathbf{x}\right) = \sum_{n=1}^{N} \chi\left(x_n\right) \tag{16}$$

  being x_n, $n = 1, ..., N$ the entries of $\mathbf{x}$, and being the auxiliary counting function χ defined as:

  $$\chi\left(n\right) = \begin{cases} 1 & if\ |c_{f,n}| > 0 \\ 0 & otherwise \end{cases} \tag{17}$$

- **Non-Zero Counting Function Thresholded** $NNZ^T\left(\mathbf{x}\right)$:

  The function $NNZ^T\left(\mathbf{x}\right)$ counts the number of non-zero coefficients of the vector $\mathbf{x}$:

$$NNZ^T(\mathbf{x}) = \sum_{n=1}^{N} \chi^T(x_n) \tag{18}$$

being x_n, $n = 1, ..., N$ the entries of $\mathbf{x}$, and being the auxiliary counting function χ^T defined as:

$$\chi^T(n) = \begin{cases} 1 & if \ |c_{f,n}| > T \\ 0 & otherwise \end{cases} \tag{19}$$

- **Sparsity Measure Function** S:

The function $S(\underline{x})$ computes the sparsity of the vector $\underline{x} = [x_1, ..., x_N]$ as:

$$S(\underline{x}) = \frac{NNZ(\underline{x})}{N} \tag{20}$$

1.4 Wavelets Definitions

- **1D Wavelet Function** φ_l^s

The(l, s)-basis function, is defined as the following:

$$\varphi_l^s(h) = \begin{cases} \psi(h) & l = 0, \ h \in [0, d_h] \\ 2^{(l-1)/2}\gamma\left(2^{(l-1)}h - sd_h\right) & l \geq 1, \ h \in [0, d_h] \\ 0 & h \notin [0, d_h] \end{cases} \quad l = 0, ..., L, \ s = 0, ..., 2^{l-1} - 1 \tag{21}$$

where d_h is the function domain dimension. The resolution level is directly related to the width of the support of $\varphi_l^s(h)$ (i.e., the finest detail representable by a wavelet function). Accordingly, the user-defined parameter L in (21) controls the resolution of the adopted basis, as well as the total number of different 1D wavelet functions that is contains (i.e., which is equal to 2^L). In (21), $\psi(h)$ and $\gamma(h)$ are the so-called *scaling* and *mother wavelet* functions, respectively, which depend on the chosen wavelet family, that comply with the following necessary conditions:

- $\int_{-\infty}^{\infty} \gamma(h)\, dh = 0$ (zero mean condition);
- $\frac{1}{d_h}\int_{-\infty}^{\infty} |\gamma(h)|^2\, dh = \frac{1}{d_h}\int_{-\infty}^{\infty} |\psi(h)|^2\, dh = 1$ (unitary energy condition).

Several wavelet families can be found in the literature, including the Ricker, the Meyer, the Shannon, the Morlet, and the Haar wavelets.

- **2D Basis Function**$\Phi_{lk}^{st}(\mathbf{r})$

The 2D (l, k, s, t)-basis function, is derived using the 1D basis functions and is defined as the following

$$\Phi_{lk}^{st}(\mathbf{r}) = \varphi_l^s(x) \times \varphi_k^t(y), \quad k = 0, ..., L, \ l = 0, ..., L, \ t = 0, ..., 2^{k-1} - 1, \ s = 0, ..., 2^{l-1} - 1 \tag{22}$$

being $\varphi_l^s(h)$, $h = x, y$, the 1D wavelet function.

- **Haar Functions** $h_k(t)$

  For the *Haar wavelet* family, the functions $\psi(h)$ and $\gamma(h)$ are respectively defined as follows

$$\psi(h) = \begin{cases} 1 & h \in [0, d_h] \\ 0 & h \notin [0, d_h] \end{cases} \tag{23}$$

  and

$$\gamma(h) = \begin{cases} 1 & h \in \left[0, \frac{d_h}{2}\right] \\ -1 & h \in \left[\frac{d_h}{2}, d_h\right] \\ 0 & h \notin [0, d_h] \end{cases} . \tag{24}$$

- **Daubechies Wavelets**

  The Daubechies wavelets are an orthogonal wavelets family, which permits to perform multi-resolution analysis of discrete functions. Daubechies wavelets are not defined in terms of scaling and wavelet functions, because there are no closed form formulas. The *cascade algorithm* is then used to compute such functions. The cascade algorithm is an iterative numerical method that starting from a set of coefficients, imitatively converges to the scaling and wavelet functions needed to perform the discrete wavelet transform.

  The filter coefficients for generating Daubechies wavelets of order 4 are:

C_0	$\frac{1+\sqrt{3}}{4\sqrt{2}}$
C_1	$\frac{3+\sqrt{3}}{4\sqrt{2}}$
C_2	$\frac{3-\sqrt{3}}{4\sqrt{2}}$
C_3	$\frac{1-\sqrt{3}}{4\sqrt{2}}$

Table 1. Daubechies-4 filter coefficients

- **Coiflet Wavelets**

  Like Daubechies wavelets, Coiflets are generated using the cascade algorithm.

- **Discrete Meyer Wavelets**

  Meyer wavelets are continuous wavelets that can be defined in the frequency domain. The discrete version of such wavelet are a discrete approximation of the Meyers wavelets, obtained using the same method used for Daubechies and Coiflets, i.e. by defining the FIR filter coefficients, and applying the cascade algorithm.

2 Wavelets

2.1 Haar

LEVEL 1

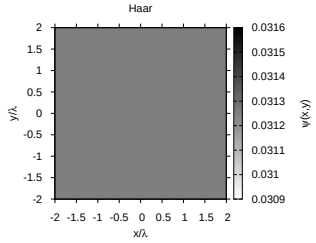

LEVEL 2

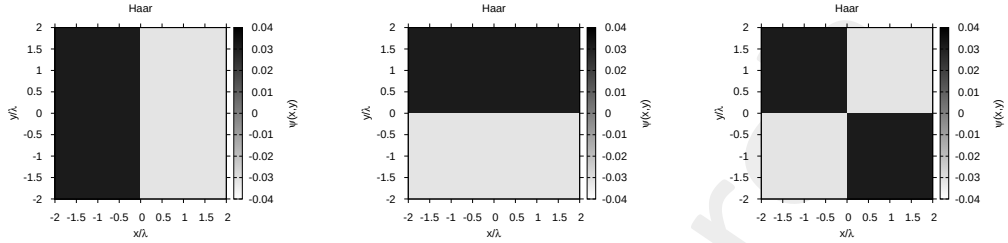

LEVEL 3

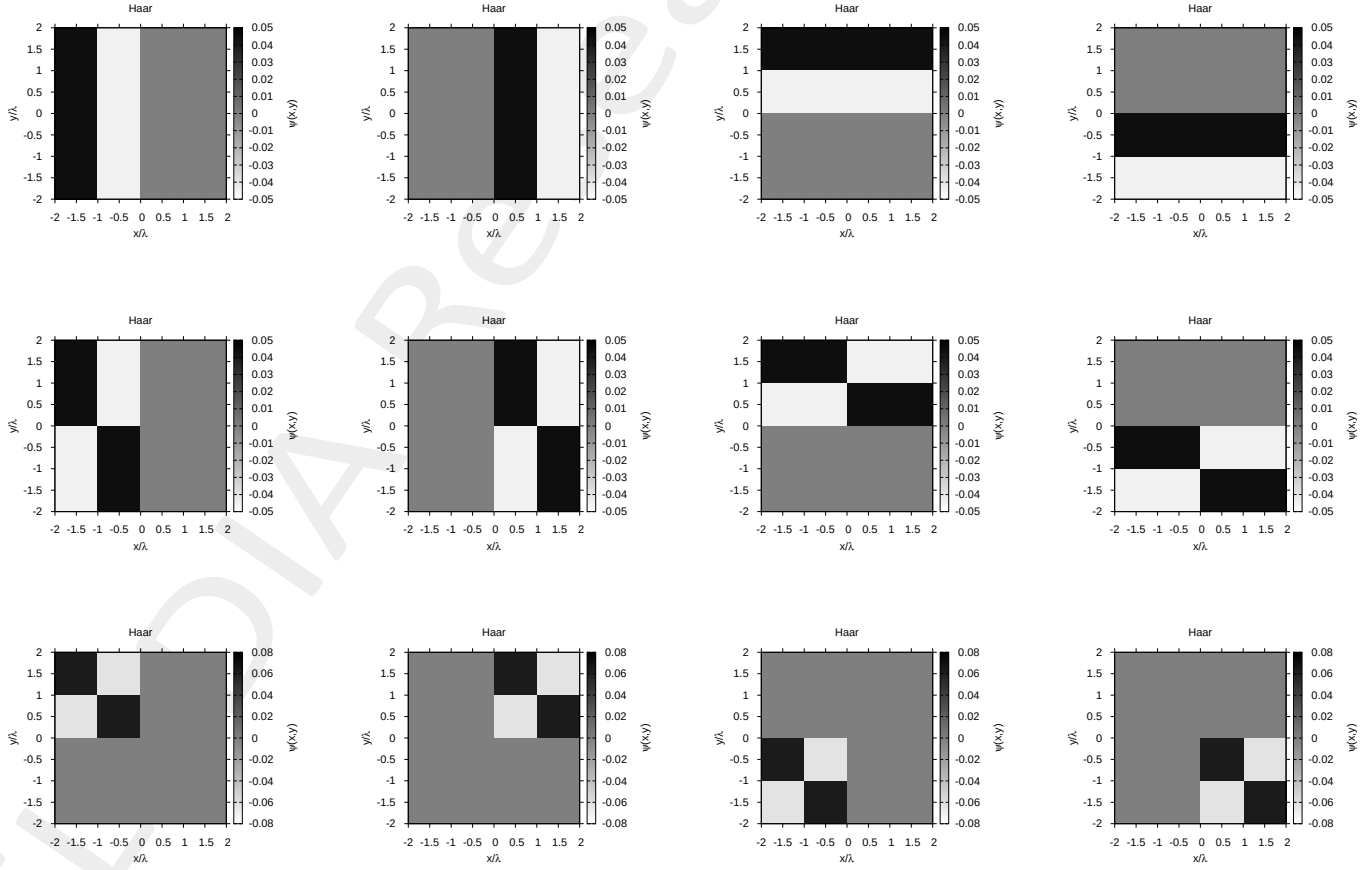

LEVEL 4

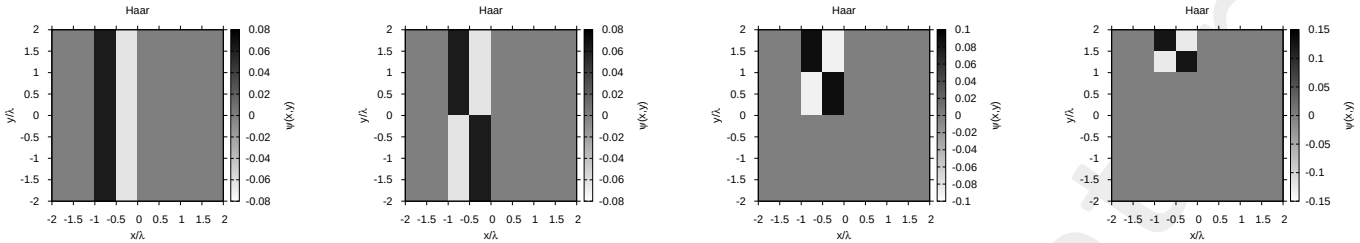

...

2.2 Daubechies-4

LEVEL 1

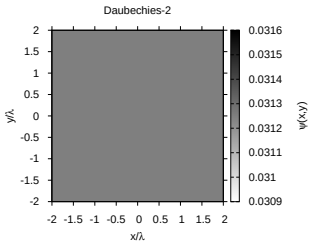

LEVEL 2

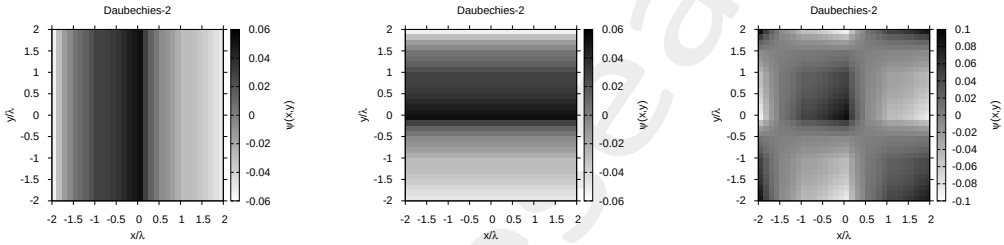

LEVEL 3

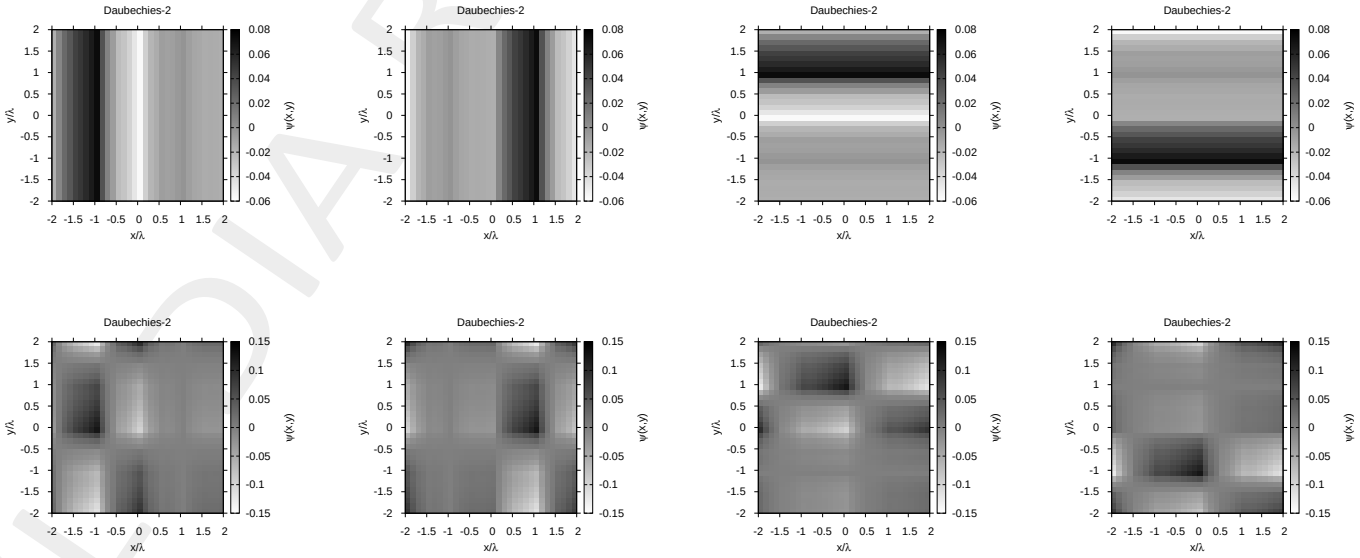

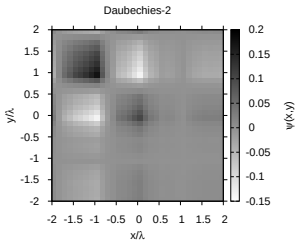

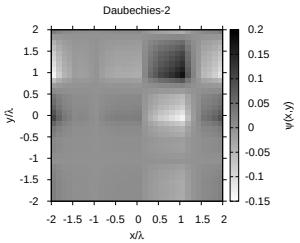

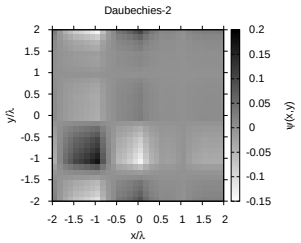

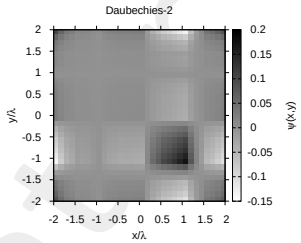

LEVEL 4

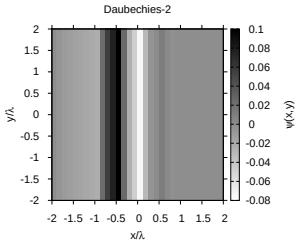

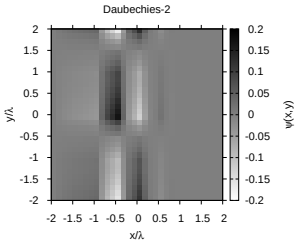

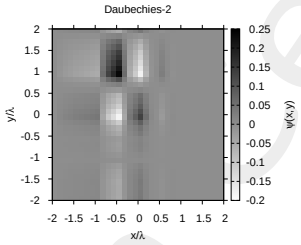

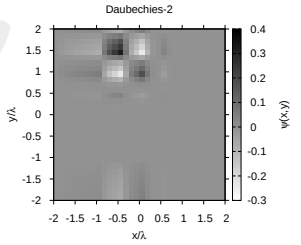

...

2.3 Daubechies-8

LEVEL 1

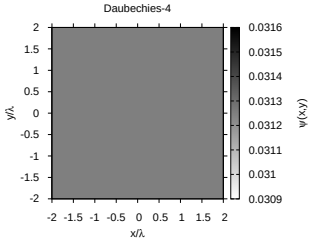

LEVEL 2

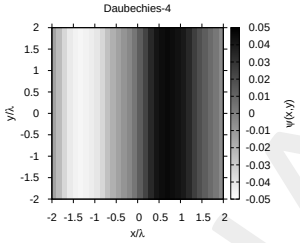

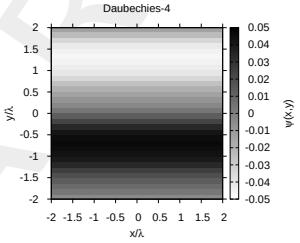

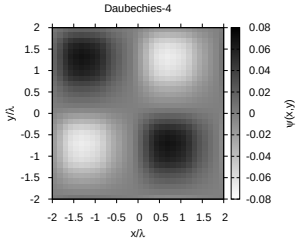

LEVEL 3

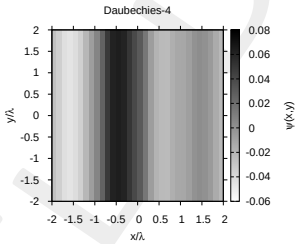

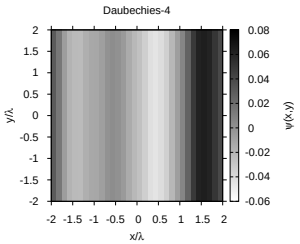

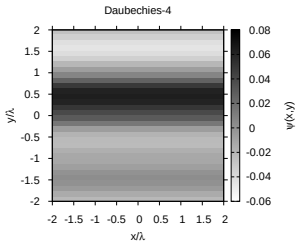

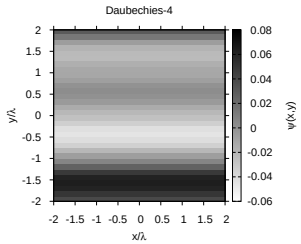

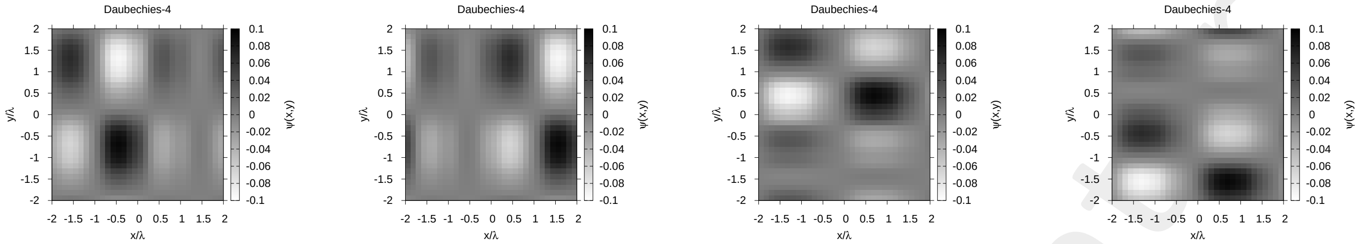

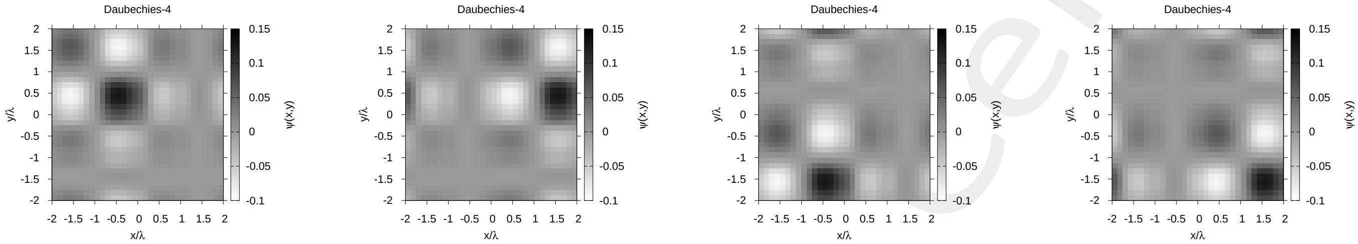

LEVEL 4

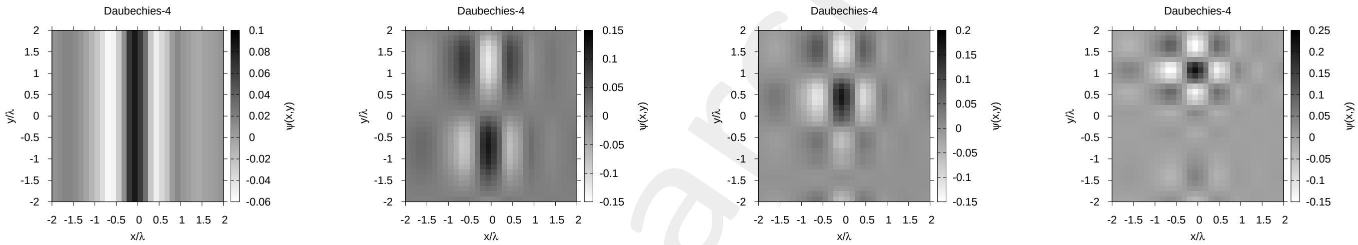

...

2.4 Coiflet-1

LEVEL 1

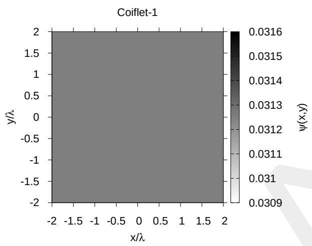

LEVEL 2

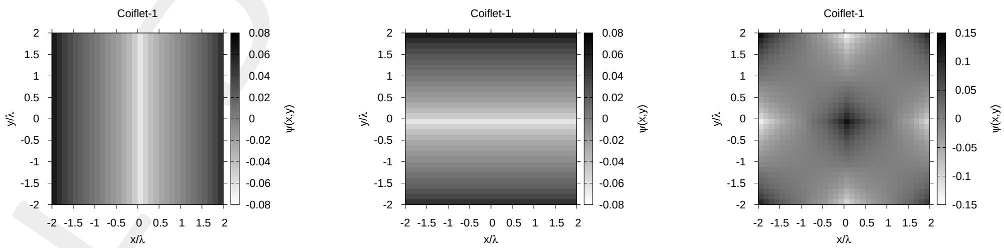

LEVEL 3

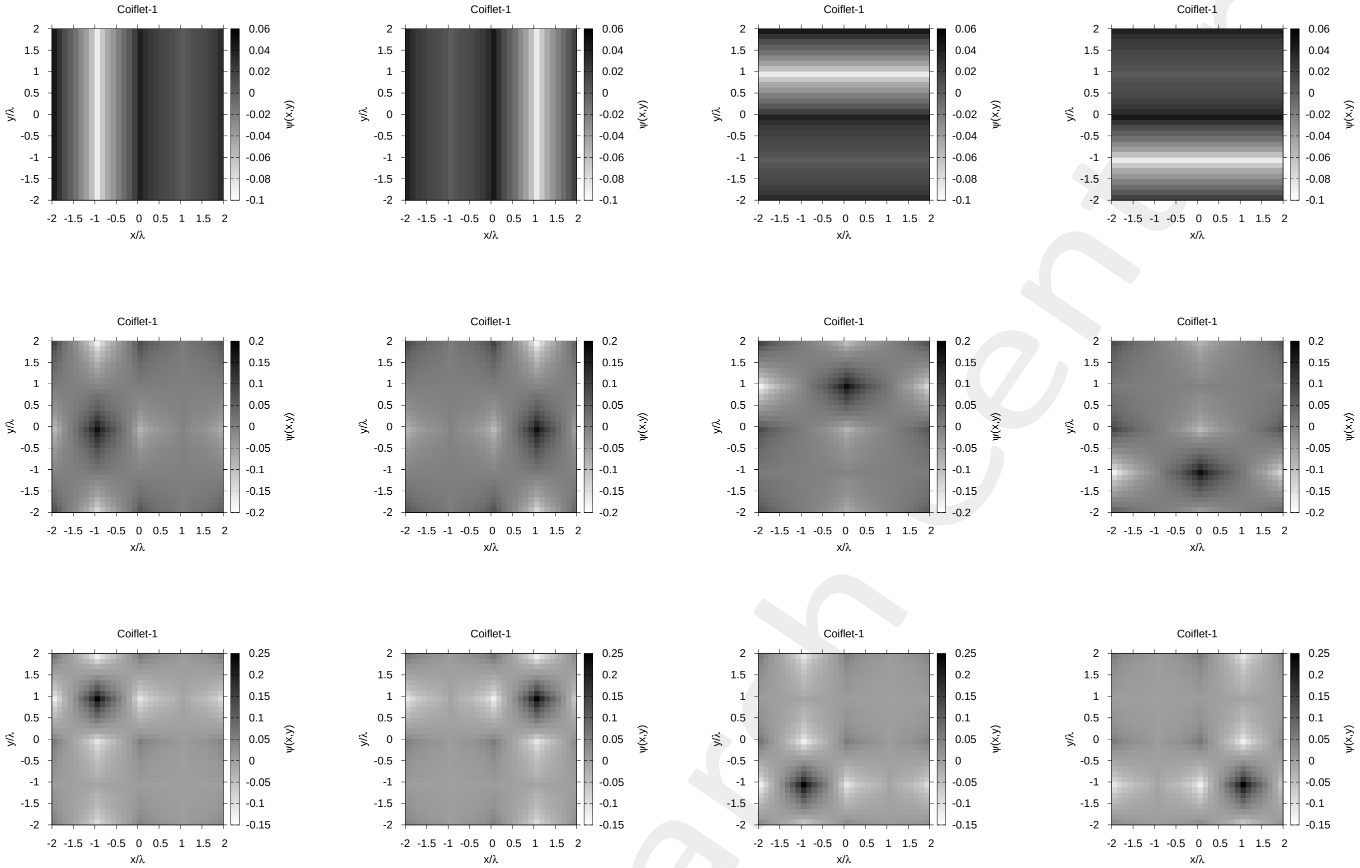

LEVEL 4

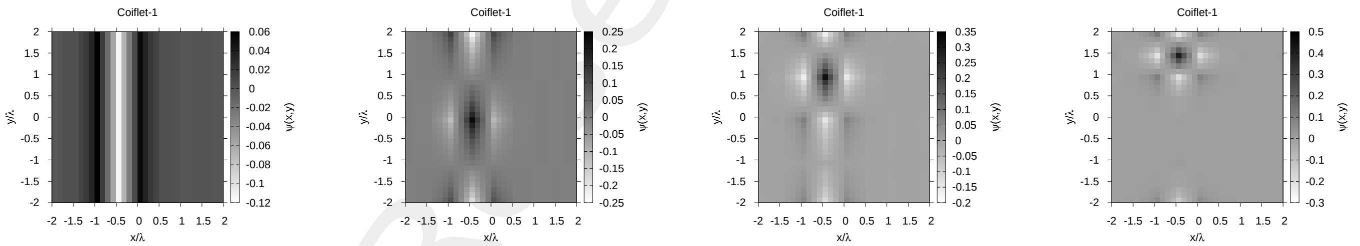

...

2.5 Coiflet-4

LEVEL 1

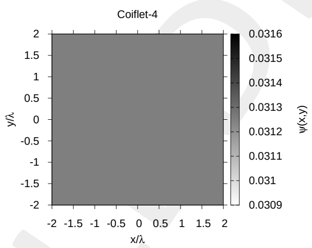

LEVEL 2

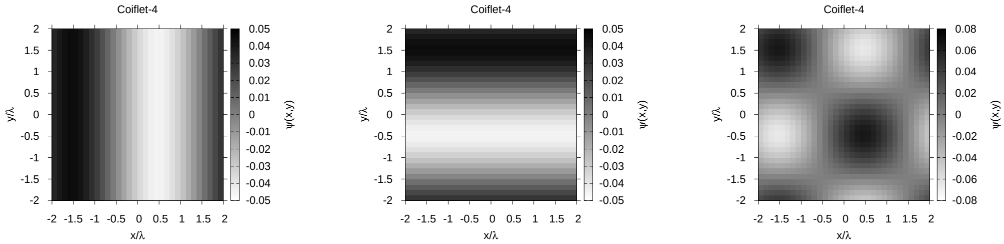

LEVEL 3

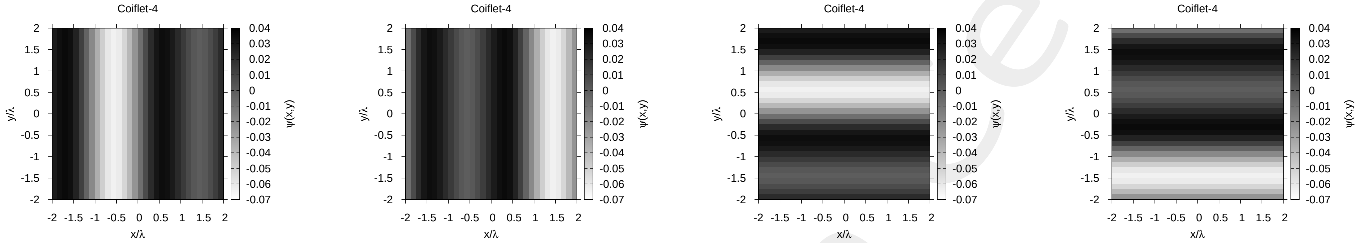

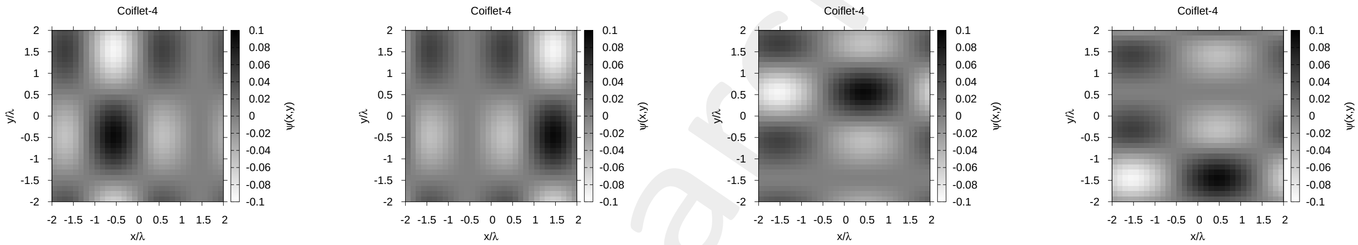

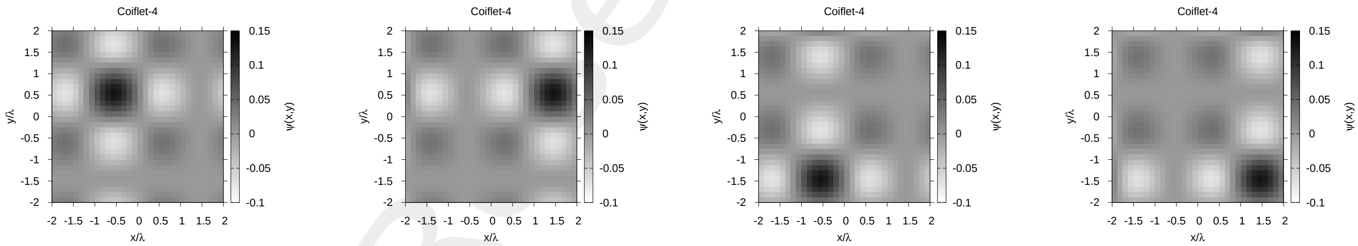

LEVEL 4

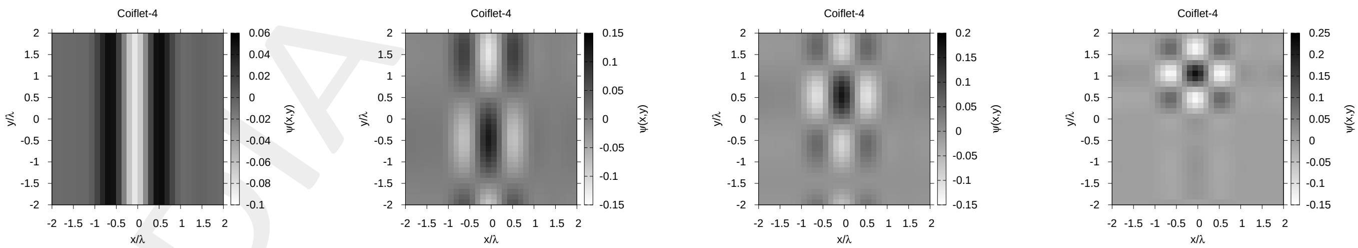

...

2.6 Discrete Meyer

LEVEL 1

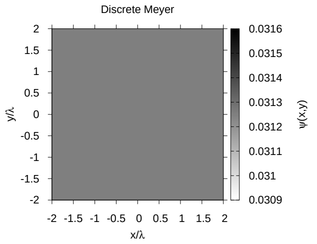

LEVEL 2

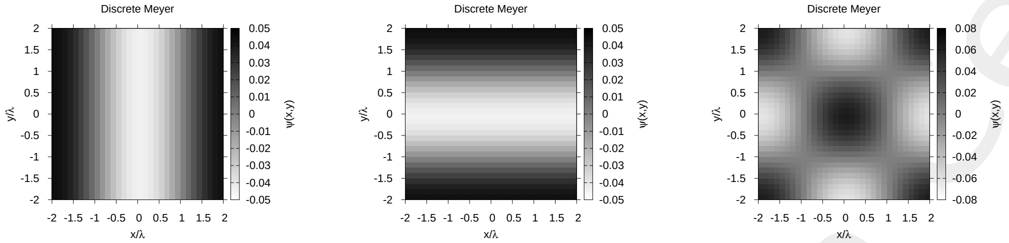

LEVEL 3

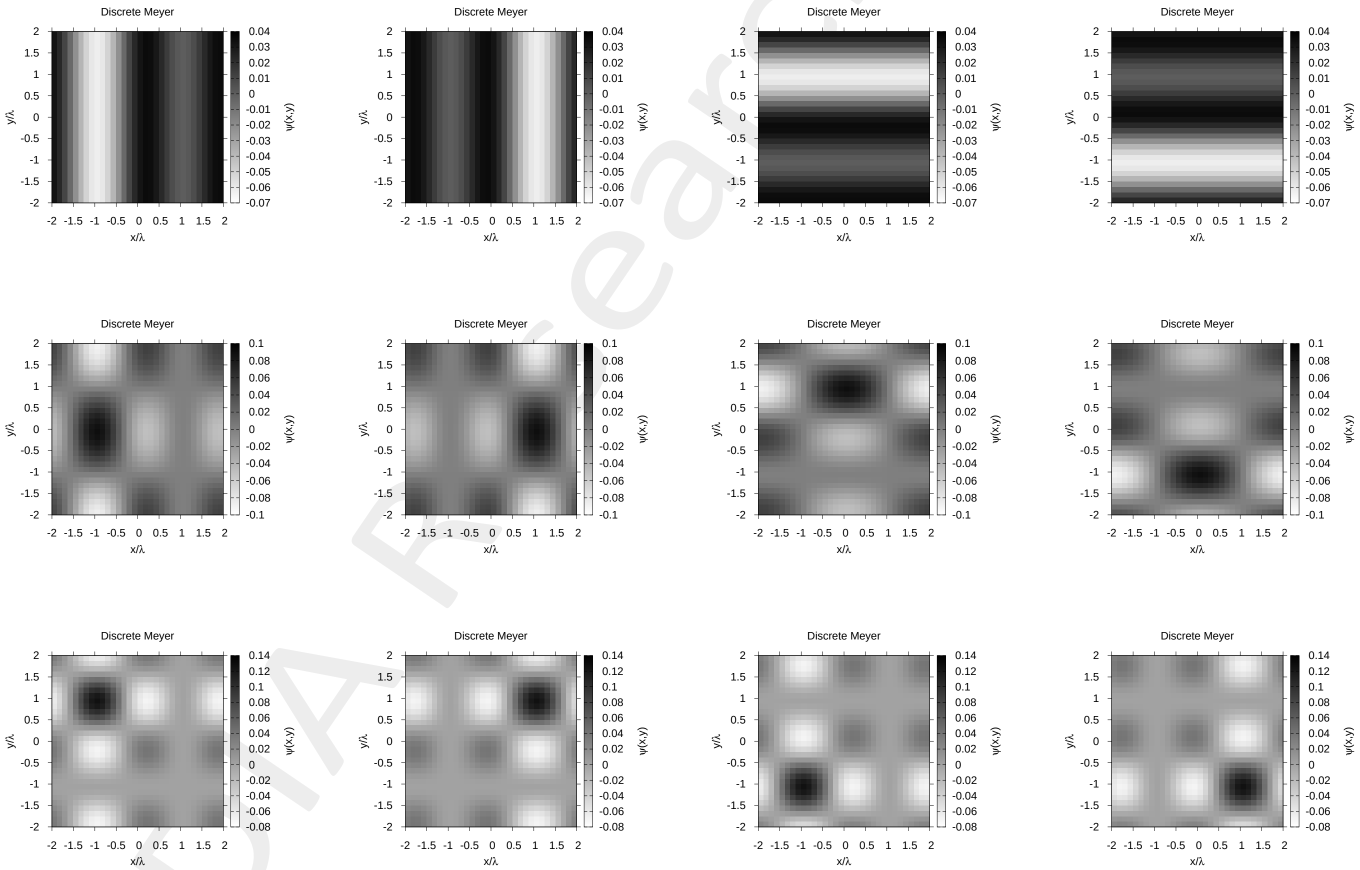

LEVEL 4

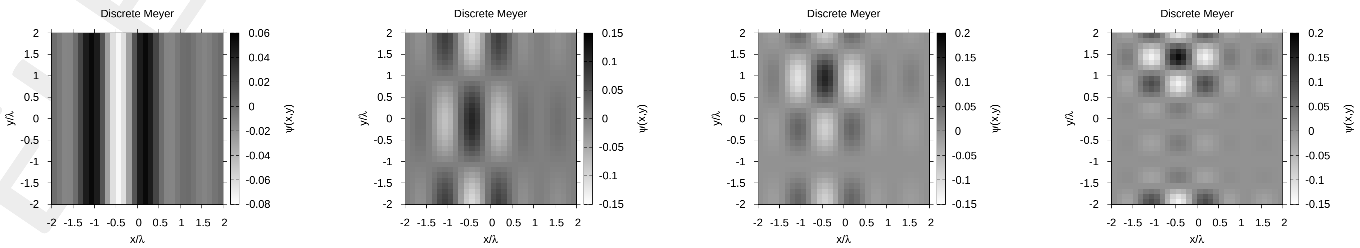

...

2.7 Exponential Basis

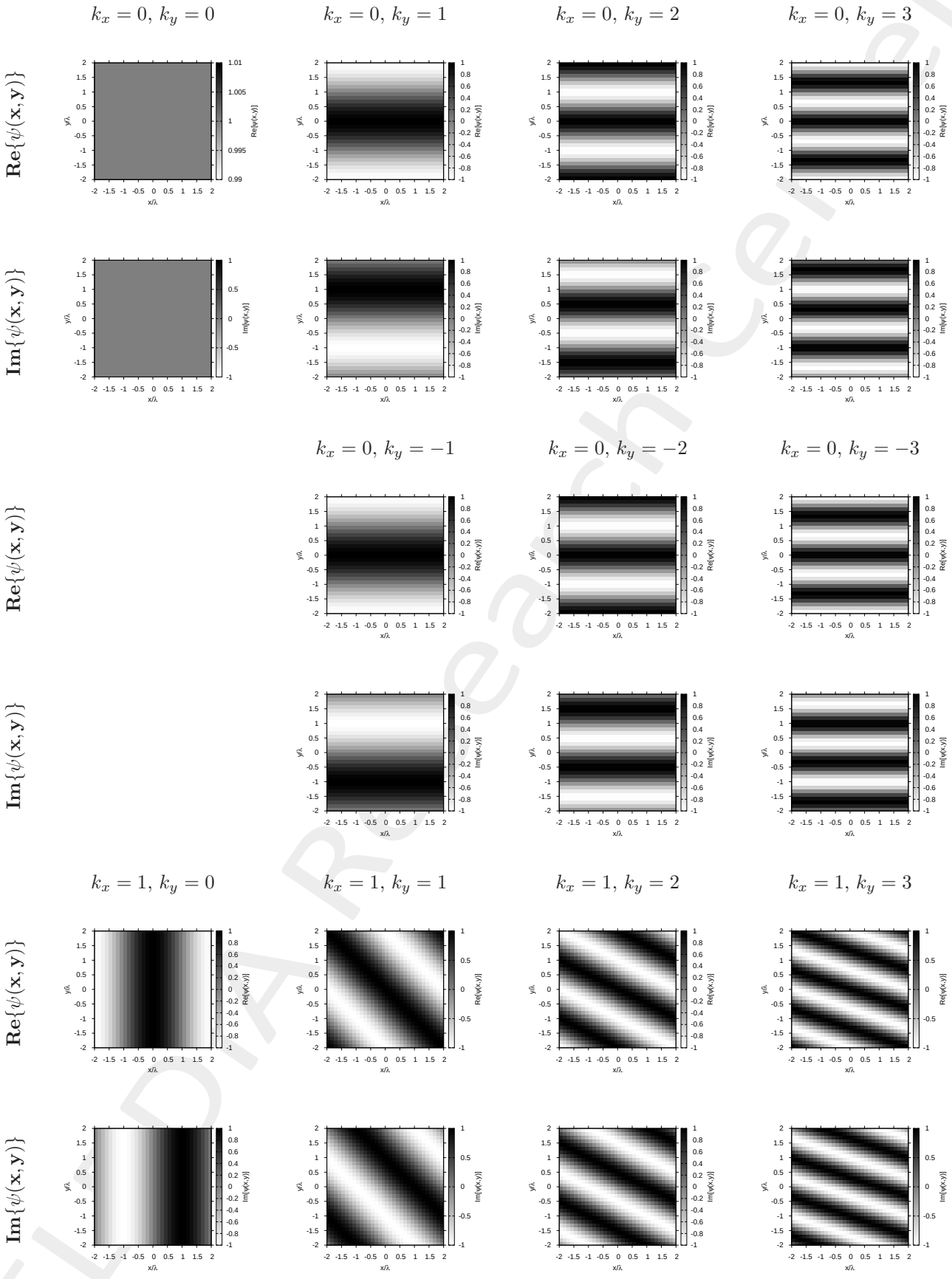

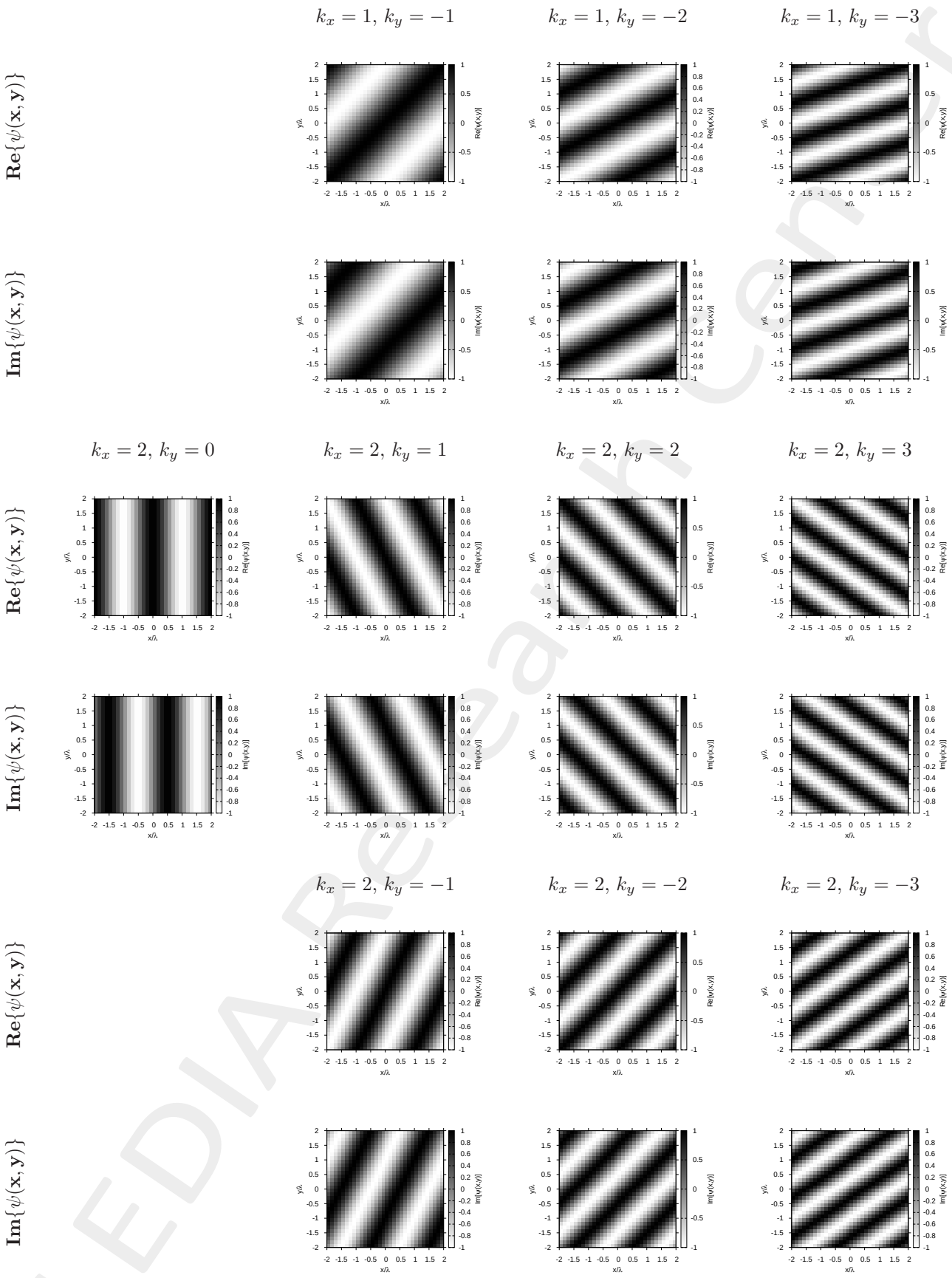

3 Numerical ResultsReconstructions:

3.1 Object Pixel #1

Goal: To prove the effectiveness of the alphabet based approach using an "ad-hoc" scatterer for pixel based domain.

Test Case Description

Object:

- $\varepsilon_{r,max} = 1.5$
- $\sigma = 0$ [S/m]
- Number of Pixels: $Nc = 21$

Sources:

- Plane waves
- Amplitude: $A = 1$
- Frequency: 300 MHz ($\lambda = 1$m)
- Number of views: $V = 36$

Direct solver:

- Square domain divided in $\sqrt{D} \times \sqrt{D}$ cells
- $D = 4096$ (64×64) $(\frac{L_D}{\sqrt{D}} = \frac{\lambda}{16})$

Investigation domain:

- Square domain divided in $\sqrt{N} \times \sqrt{N}$ cells
- $N = 1024$ (32×32) $(\frac{L_D}{\sqrt{N}} = \frac{\lambda}{8})$
- $L_D = 4\lambda$

Measurement domain:

- Measurement points taken on a circle of radius $\rho = 4\lambda$
- $M = 36$

M-BCS parameters:

- $a = 1.0 \times 10^{-2}$
- $b = 1.0 \times 10^{-5}$

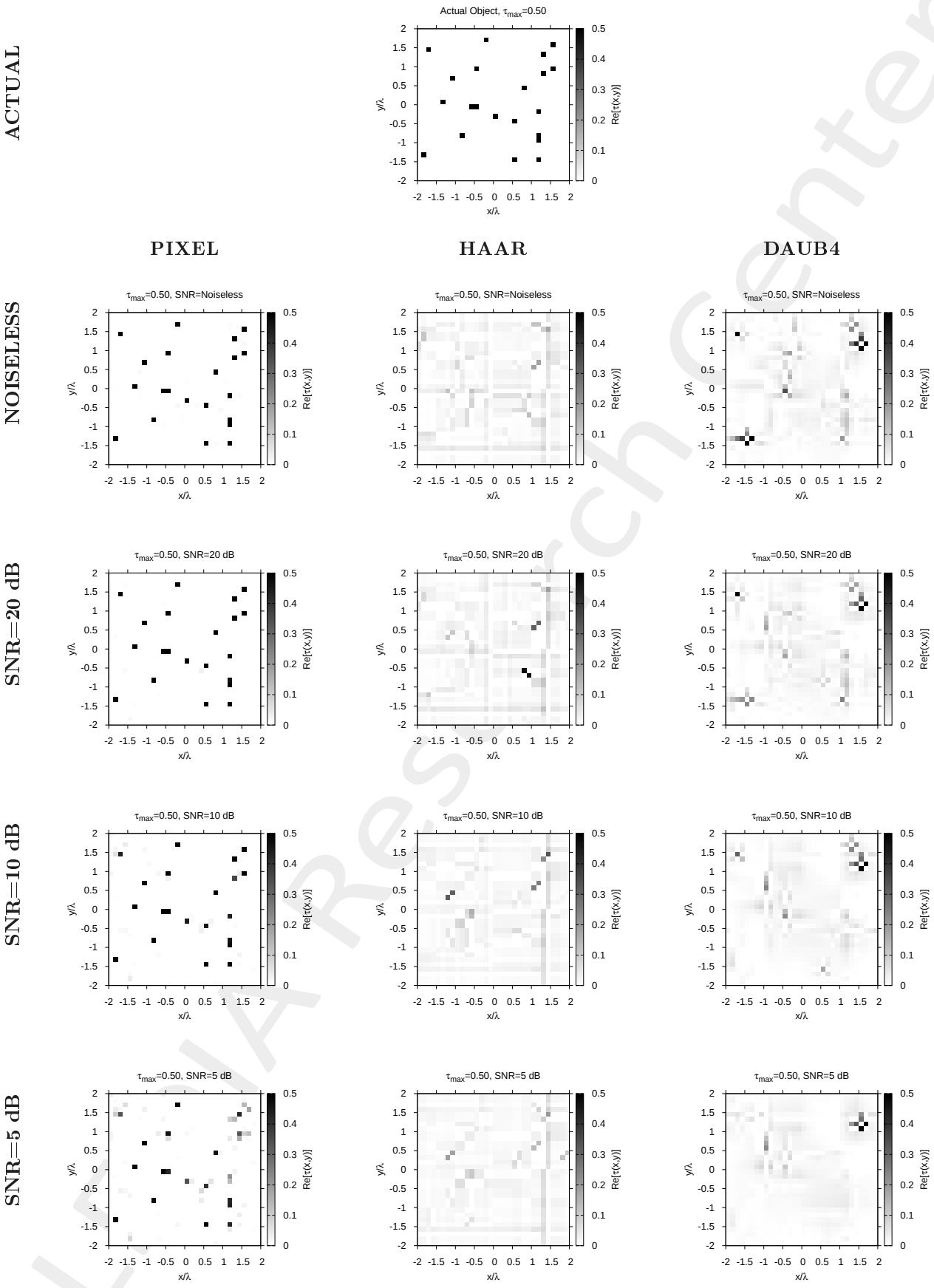

Figure 1: Actual and retrieved object considering different wavelet expansions.

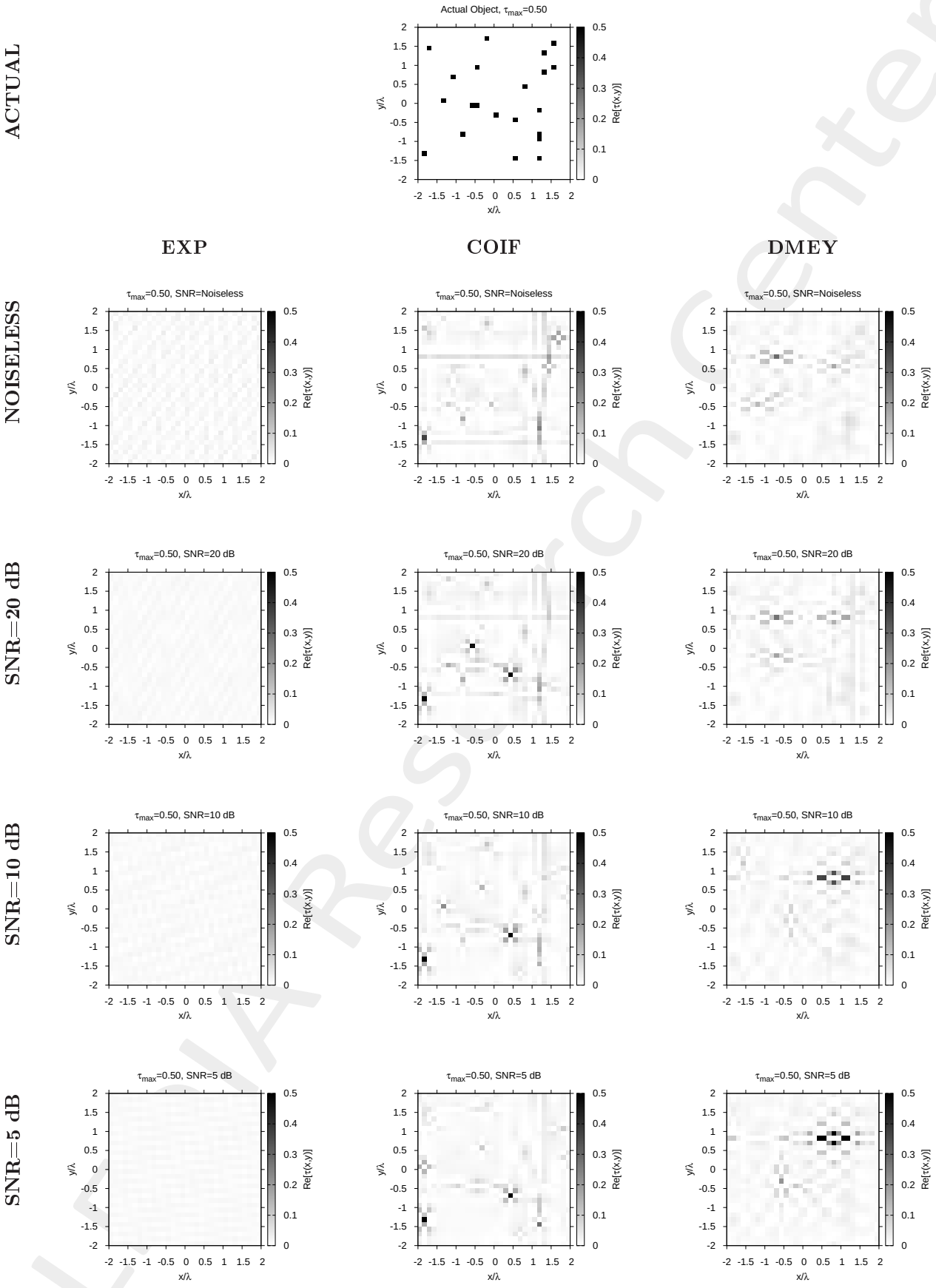

Figure 2: Actual and retrieved object considering different wavelet expansions.

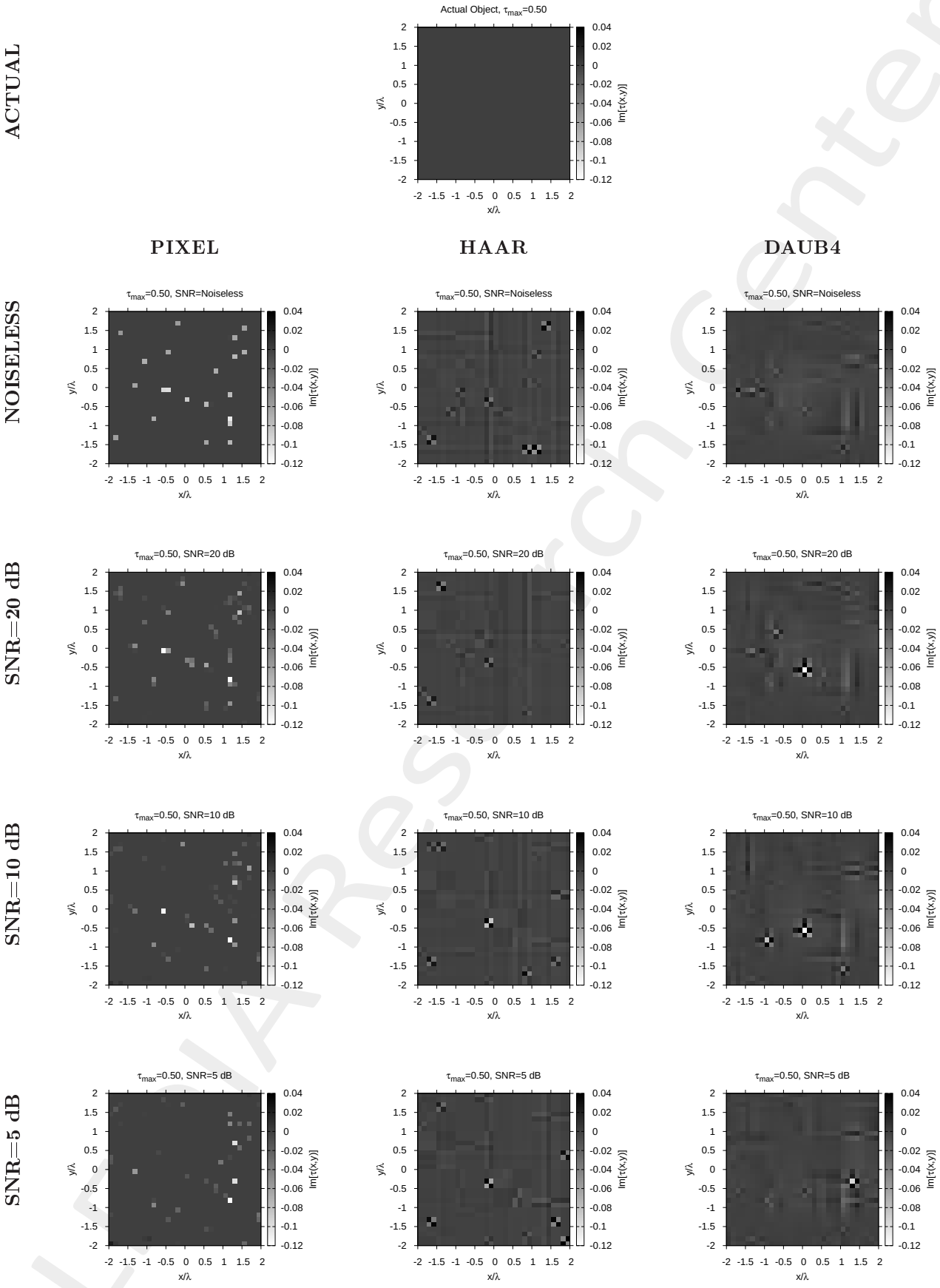

Figure 3: Actual and retrieved object considering different wavelet expansions.

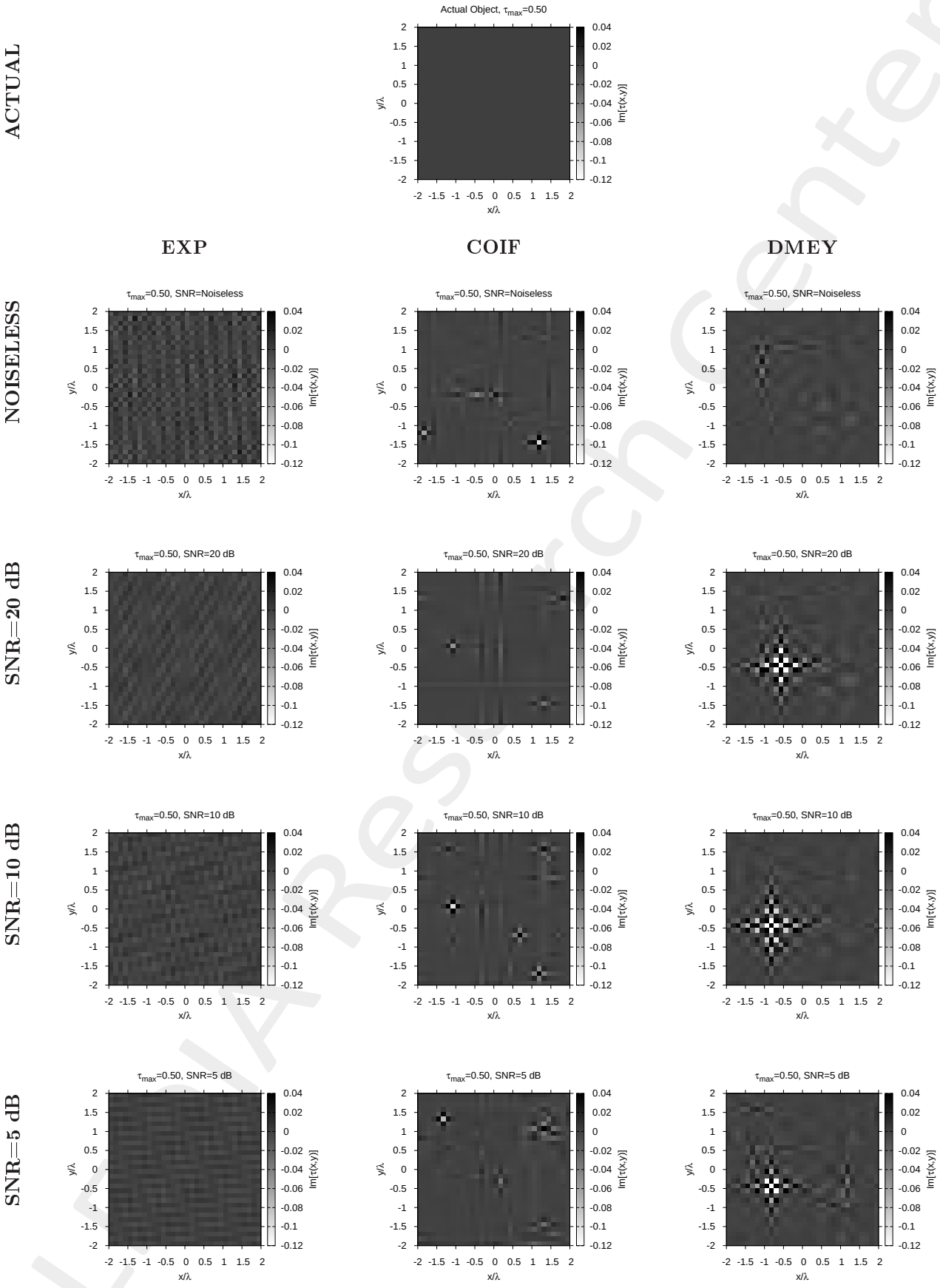

Figure 4: Actual and retrieved object considering different wavelet expansions.

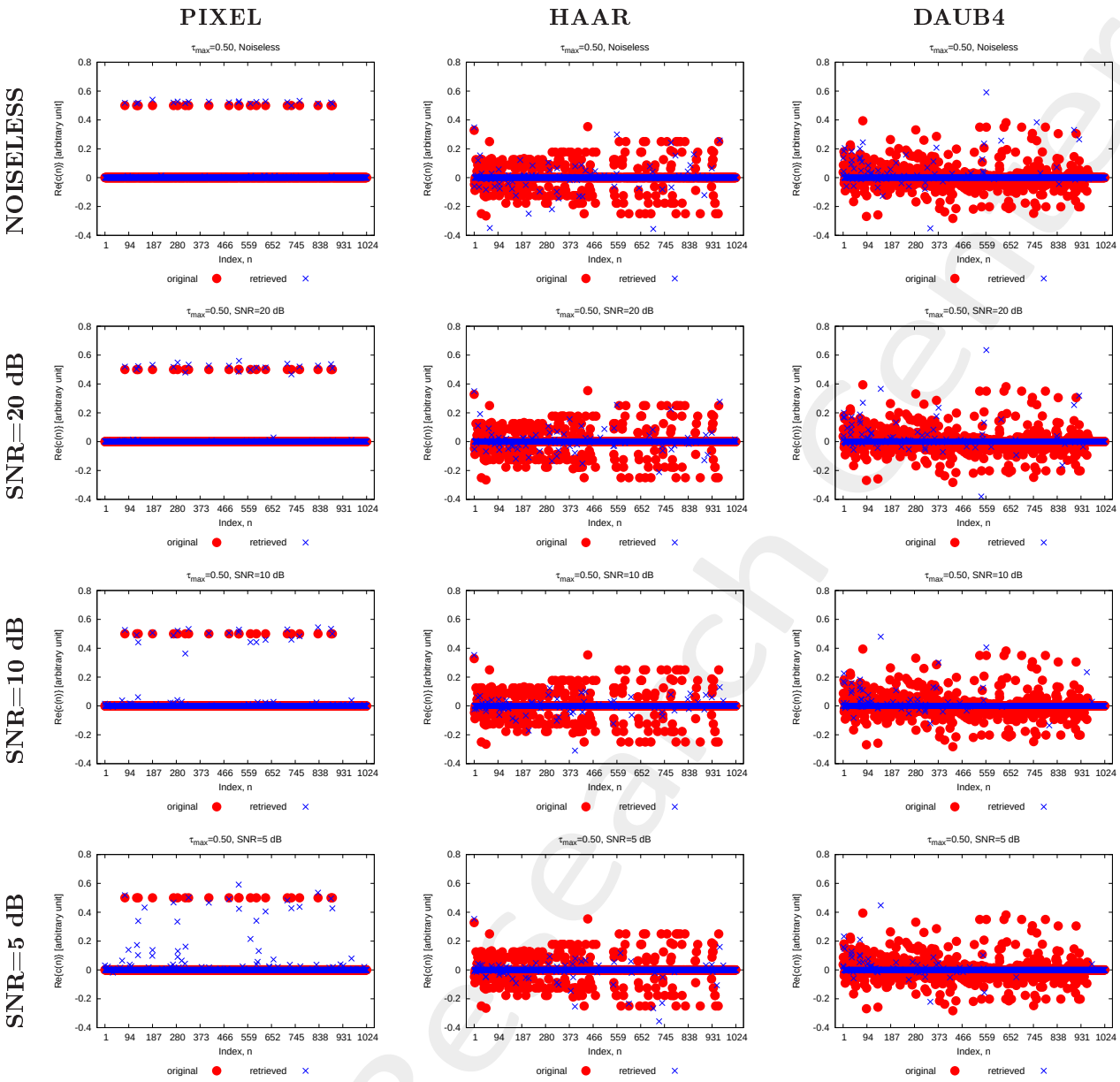

Figure 5: Real part of the actual and retrieved coefficients considering different wavelet expansions.

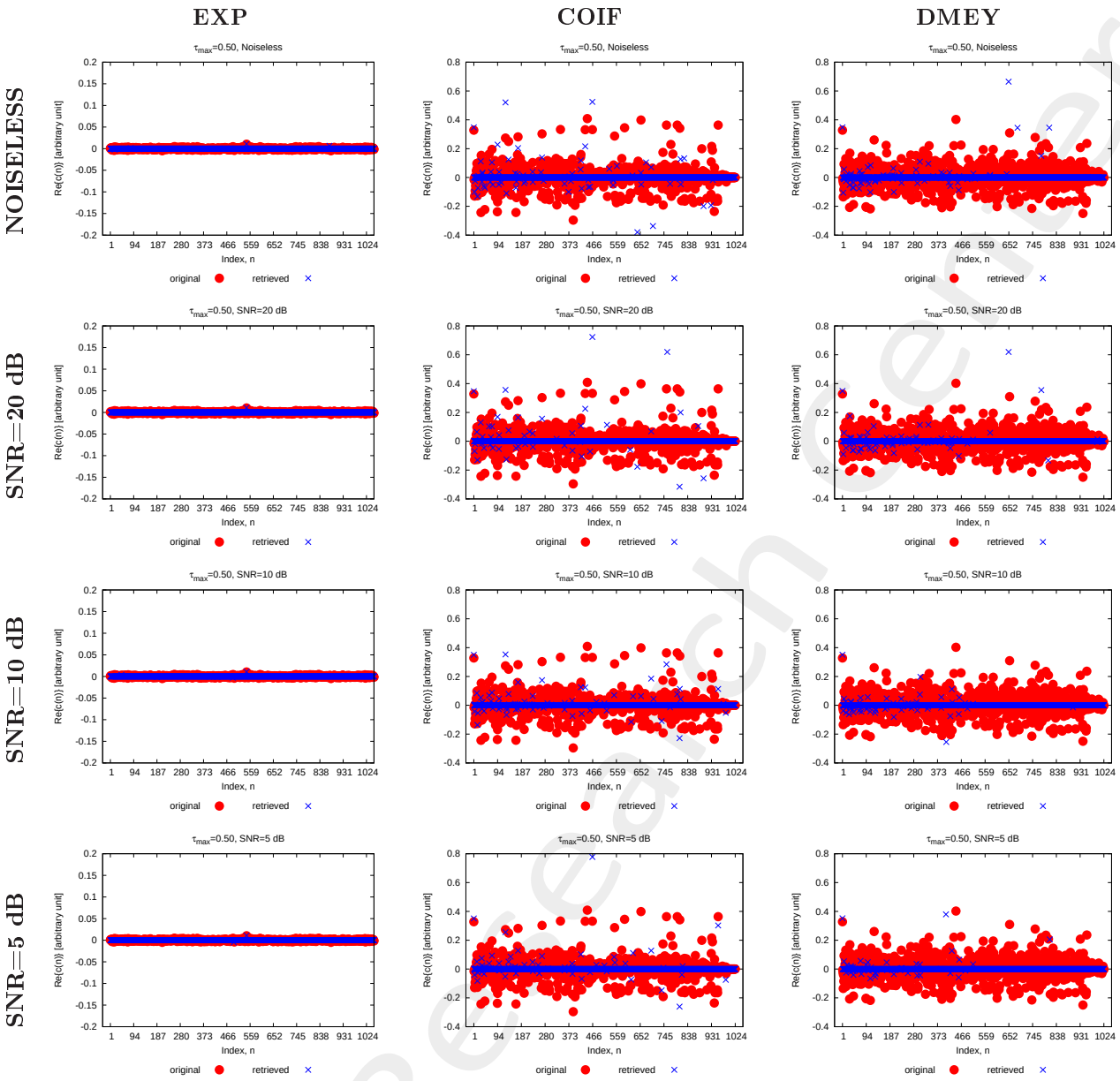

Figure 6: Real part of the actual and retrieved coefficients considering different wavelet expansions.

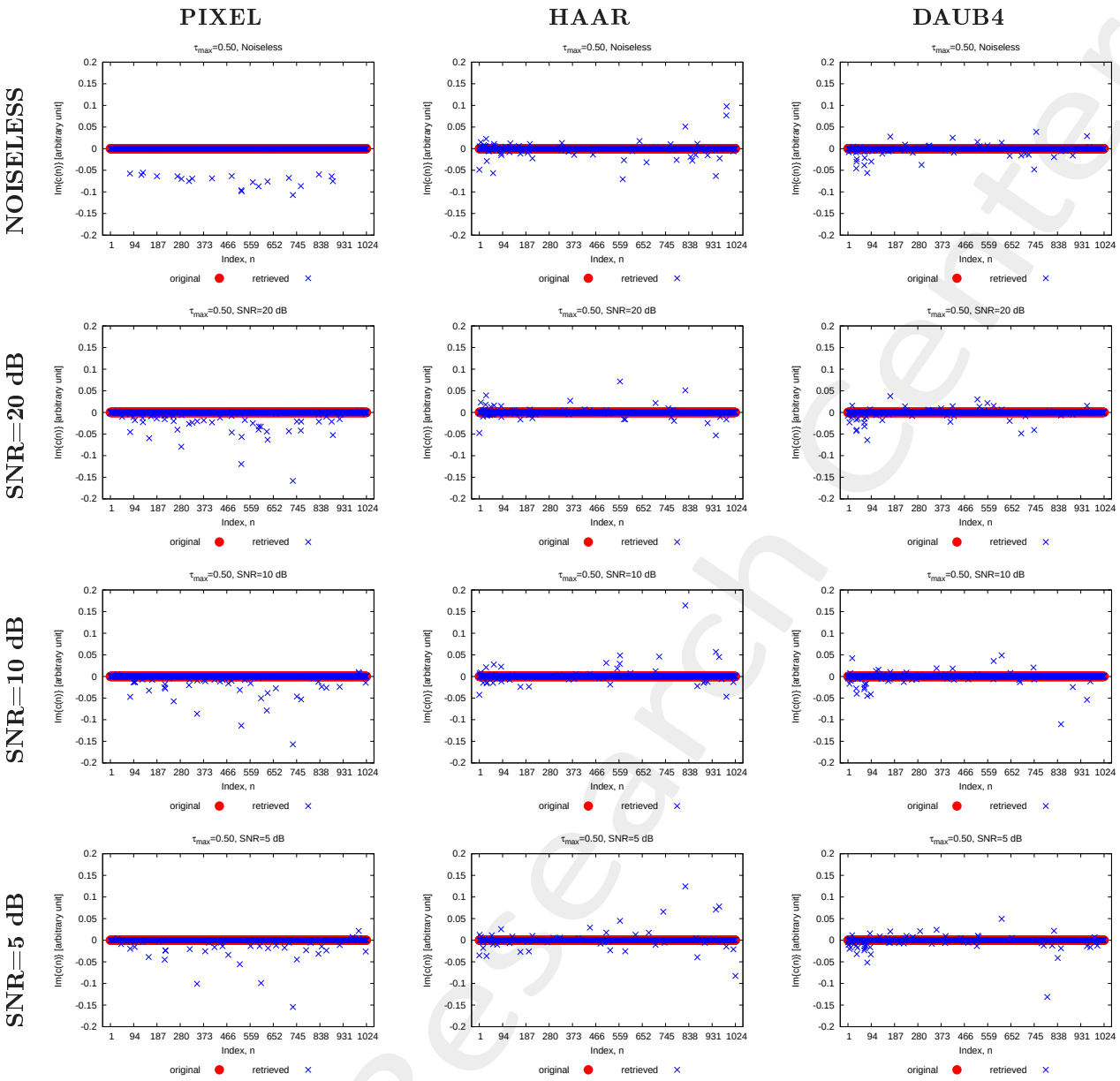

Figure 7: Imaginary part of the actual and retrieved coefficients considering different wavelet expansions.

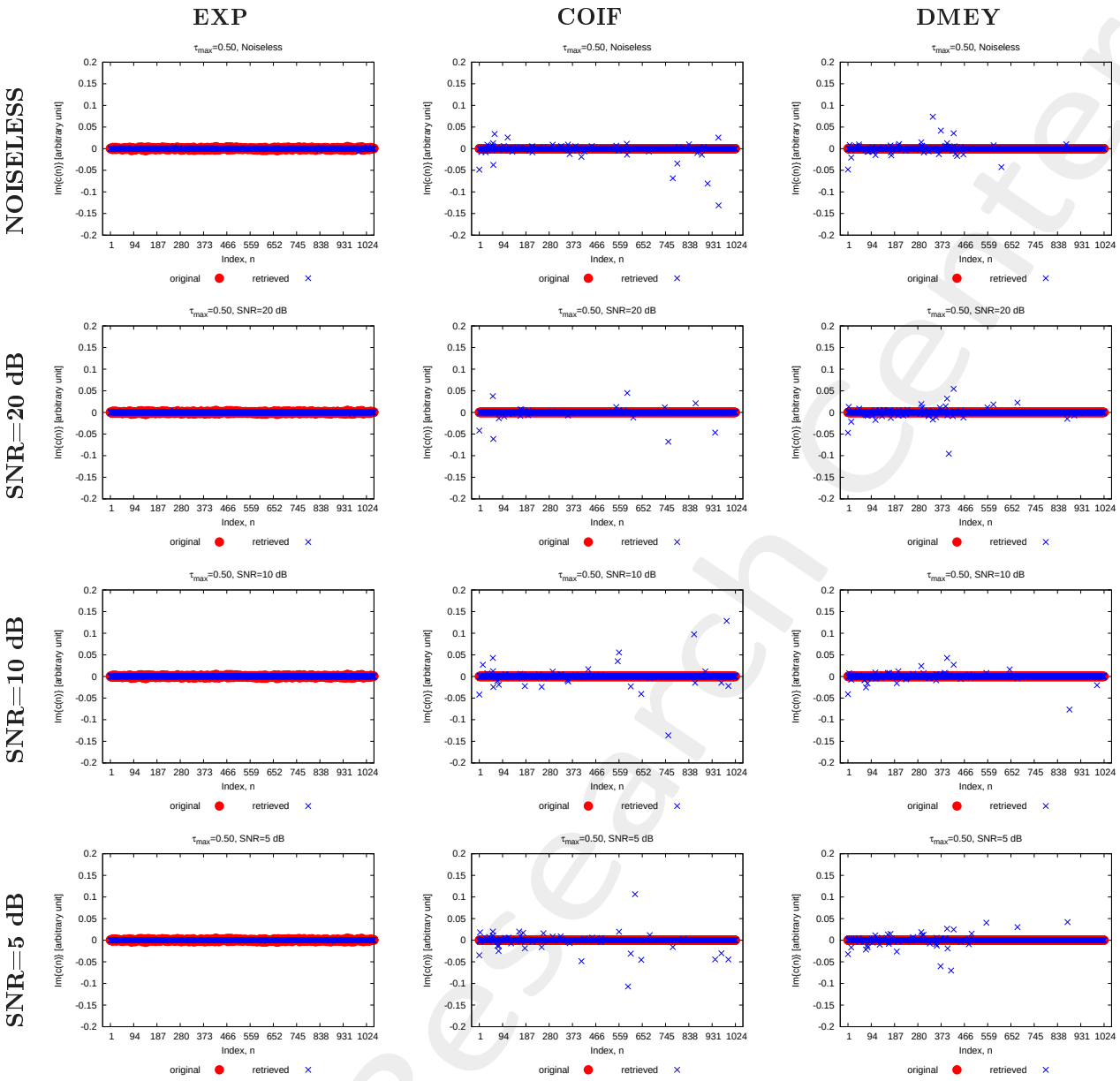

Figure 8: Imaginary part of the actual and retrieved coefficients considering different wavelet expansions.

Coefficients Analysis $T = 100\%$:

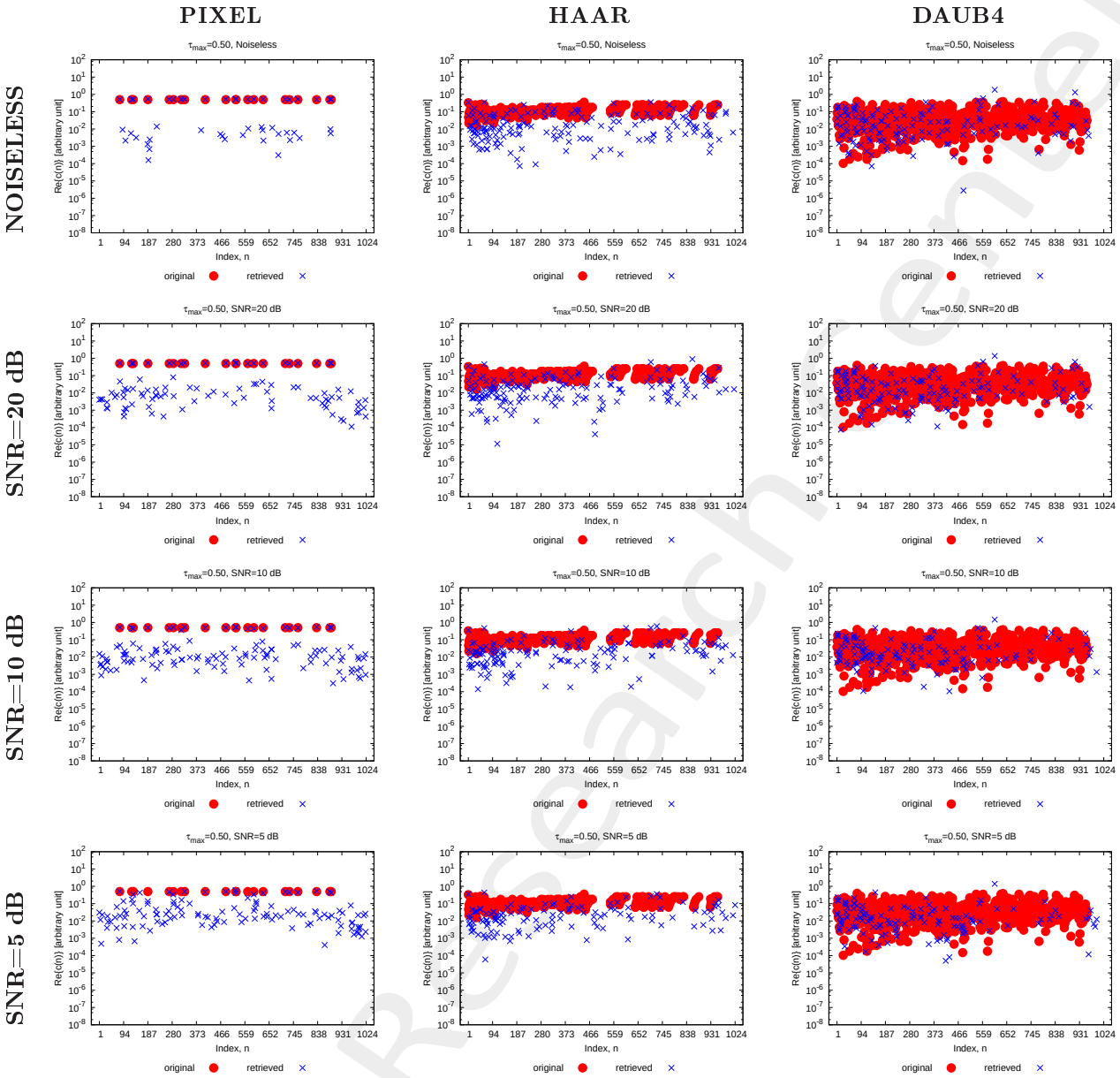

Figure 9: Absolute value [dB] of the actual and retrieved coefficients considering different wavelet expansions.

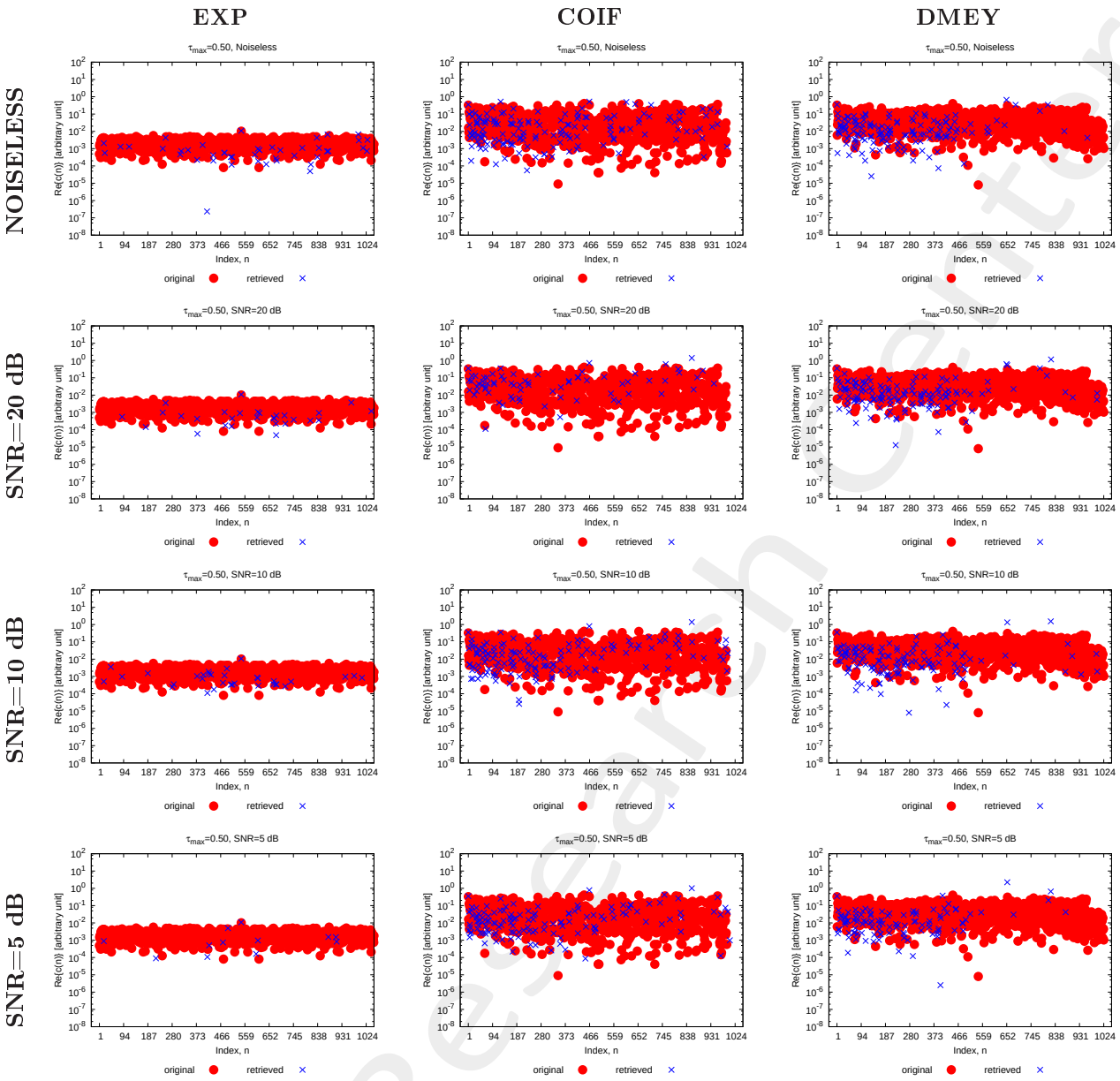

Figure 10: Absolute value [dB] of the actual and retrieved coefficients considering different wavelet expansions.

$T = 100\%$

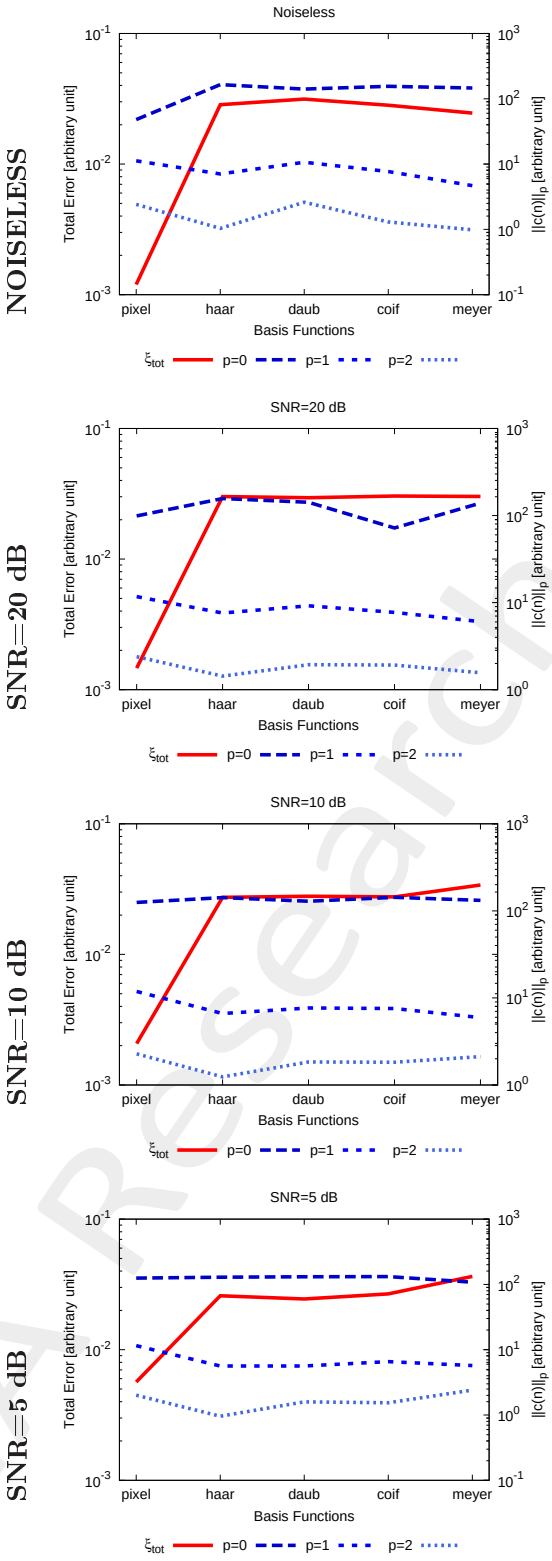

Figure 11: $[T = 100\%]$ - Comparison of ξ_{tot}, and L_0, L_1, L_2 Norms of the retrieved basis expansion coefficients, for each alphabet basis.

	$L_0 - norm$					
SNR [dB]	$Pixel$	$Haar$	$Daub4$	$Coiflet$	$DMeyer$	Exp
$Actual$	21	299	706	877	1024	1024
$Noiseless$	**48**	165	141	155	146	42
20	99	157	142	**72**	139	28
10	**125**	142	129	143	132	33
5	125	129	131	132	**108**	12
	$L_1 - norm$					
SNR [dB]	$Pixel$	$Haar$	$Daub4$	$Coiflet$	$DMeyer$	Exp
$Actual$	10.5	35.2	39.1	41.2	50.8	2.02
$Noiseless$	11.2	7.10	10.68	7.68	4.68	5.9×10^{-2}
20	11.7	7.60	9.19	7.71	6.04	3.1×10^{-2}
10	11.87	6.67	7.67	7.55	5.94	3.9×10^{-2}
5	11.54	5.63	5.63	6.57	5.72	2.3×10^{-2}
	$L_2 - norm$					
SNR [dB]	$Pixel$	$Haar$	$Daub4$	$Coiflet$	$DMeyer$	Exp
$Actual$	2.29	2.29	2.29	2.29	2.29	7.2×10^{-2}
$Noiseless$	2.41	1.04	2.60	1.30	0.99	1.7×10^{-2}
20	2.39	1.43	1.93	1.92	1.57	1.2×10^{-2}
10	2.27	1.24	1.84	1.83	2.12	1.3×10^{-2}
5	2.01	0.96	1.59	1.54	2.41	1.2×10^{-2}

Table 1: $[T = 100\%]$ - Number of the retrieved non-zero coefficients ($L_0 - norm$), $L_1 - norm$, and $L_2 - norm$ using different wavelet functions.

Thresholded Analysis:

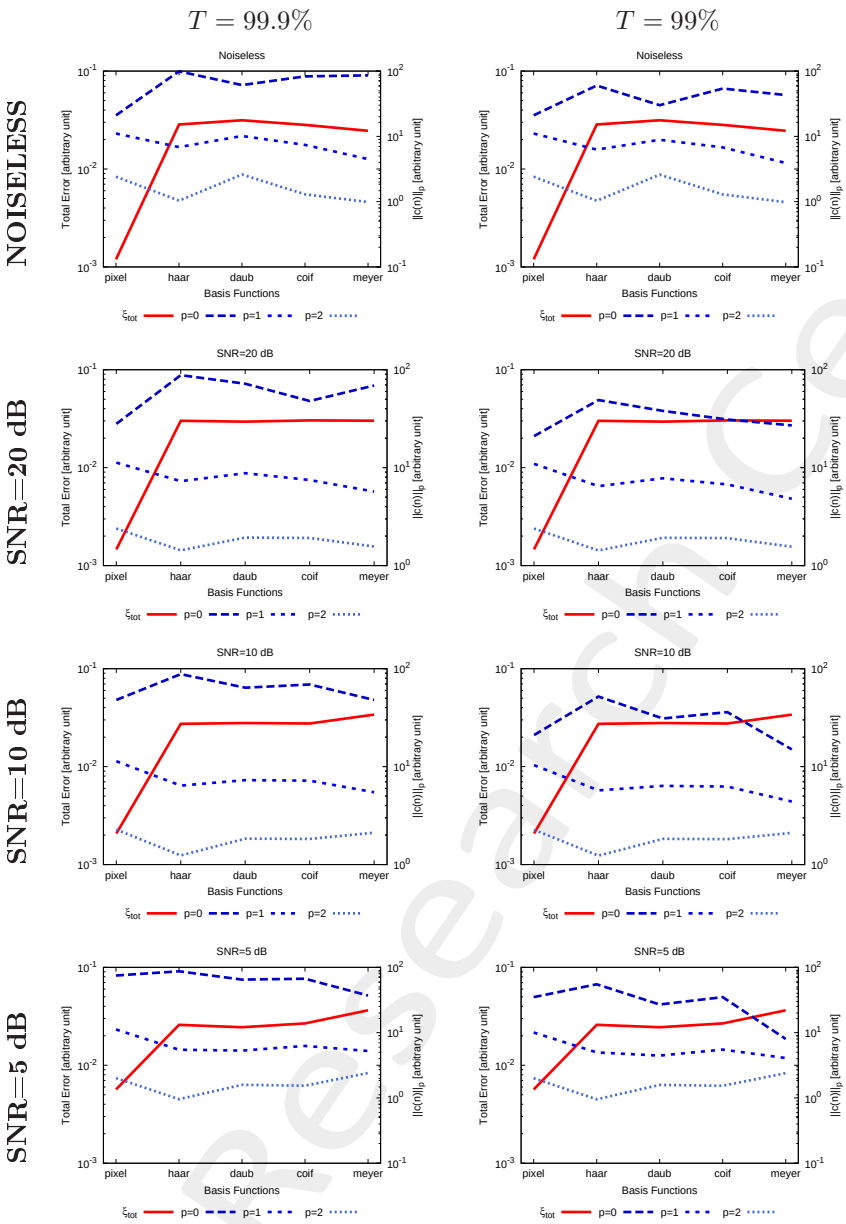

Figure 12: Comparison of ξ_{tot}, and L_0, L_1, L_2 Norms of the retrieved basis expansion coefficients, for each alphabet basis.

	$L_0 - norm$				
SNR [dB]	$Pixel$	$Haar$	$Daub4$	$Coiflet$	$DMeyer$
$Actual$	21	299	706	877	1024
$Noiseless$	21	99	61	83	86
20	28	88	72	48	69
10	48	88	64	69	48
5	75	87	65	67	37
	$L_1 - norm$				
SNR [dB]	$Pixel$	$Haar$	$Daub4$	$Coiflet$	$DMeyer$
$Actual$	10.5	35.2	39.1	41.2	50.8
$Noiseless$	11.05	6.84	10.12	7.41	4.49
20	11.26	7.28	8.79	7.48	5.70
10	11.36	6.40	7.28	7.19	5.48
5	11.19	5.47	5.31	6.27	5.23
	$L_2 - norm$				
SNR [dB]	$Pixel$	$Haar$	$Daub4$	$Coiflet$	$DMeyer$
$Actual$	2.29	2.29	2.29	2.29	2.29
$Noiseless$	2.41	1.03	2.60	1.30	0.99
20	2.39	1.43	1.93	1.92	1.57
10	2.27	1.24	1.84	1.83	2.12
5	2.01	0.96	1.59	1.54	2.40

Table 2: $[T = 99.9\%]$ - Number of the retrieved non-zero coefficients ($L_0 - norm$), $L_1 - norm$, and $L_2 - norm$ using different wavelet functions.

	$L_0 - norm$				
SNR [dB]	$Pixel$	$Haar$	$Daub4$	$Coiflet$	$DMeyer$
$Actual$	21	299	706	877	1024
$Noiseless$	21	60	30	54	43
20	21	49	38	32	27
10	21	52	31	36	15
5	35	55	27	35	8
	$L_1 - norm$				
SNR [dB]	$Pixel$	$Haar$	$Daub4$	$Coiflet$	$DMeyer$
$Actual$	10.5	35.2	39.1	41.2	50.8
$Noiseless$	11.06	6.27	8.85	6.79	3.92
20	10.94	6.47	7.79	6.75	4.81
10	10.35	5.73	6.36	6.26	4.4
5	10.06	4.98	4.45	5.50	4.09
	$L_2 - norm$				
SNR [dB]	$Pixel$	$Haar$	$Daub4$	$Coiflet$	$DMeyer$
$Actual$	2.29	2.29	2.29	2.29	2.29
$Noiseless$	2.41	1.03	2.59	1.29	0.98
20	2.39	1.43	1.92	1.91	1.56
10	2.27	1.23	1.83	1.82	2.11
5	2.00	0.95	1.58	1.53	2.40

Table 3: $[T = 99\%]$ - Number of the retrieved non-zero coefficients ($L_0 - norm$), $L_1 - norm$, and $L_2 - norm$ using different wavelet functions.

Resume:

	$T = 100\%$				
SNR [dB]	$Pixel$	$Haar$	$Daub4$	$Coiflet$	$DMeyer$
$Noiseless$	**48**	165	141	155	146
20	99	157	142	**72**	139
10	**125**	142	129	143	132
5	125	129	131	132	**108**
	$T = 99.9\%$				
SNR [dB]	$Pixel$	$Haar$	$Daub4$	$Coiflet$	$DMeyer$
$Noiseless$	**21**	99	61	83	86
20	**28**	88	72	48	69
10	**48**	88	64	69	**48**
5	75	87	65	67	**37**
	$T = 99\%$				
SNR [dB]	$Pixel$	$Haar$	$Daub4$	$Coiflet$	$DMeyer$
$Noiseless$	**21**	60	30	54	43
20	**21**	49	38	32	27
10	21	52	31	36	**15**
5	35	55	27	35	**8**

Table 4: $L_0 - norm$.

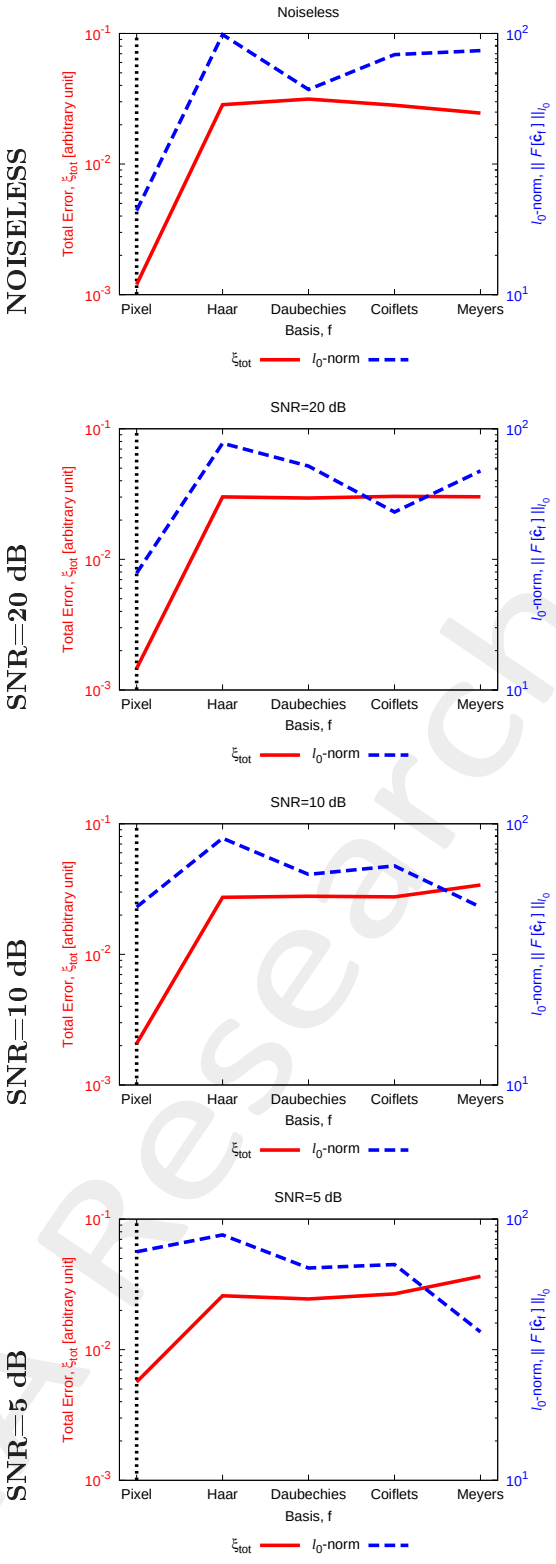

Figure 13: $L_0 - norm$ vs Total Error, considering $T = 99.9\%$.

Comparison SoA:

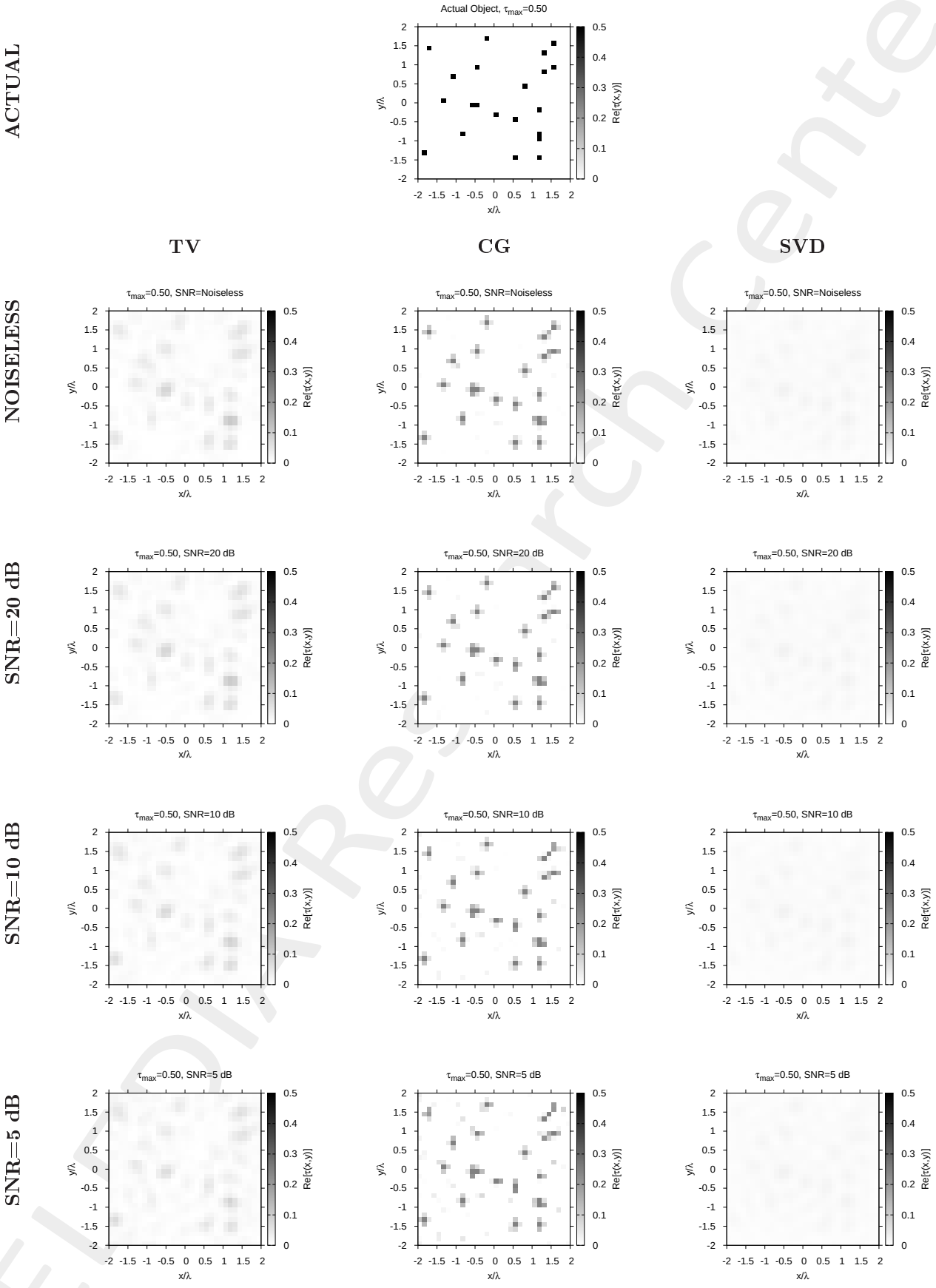

Figure 14: Actual and retrieved object considering different wavelet expansions.

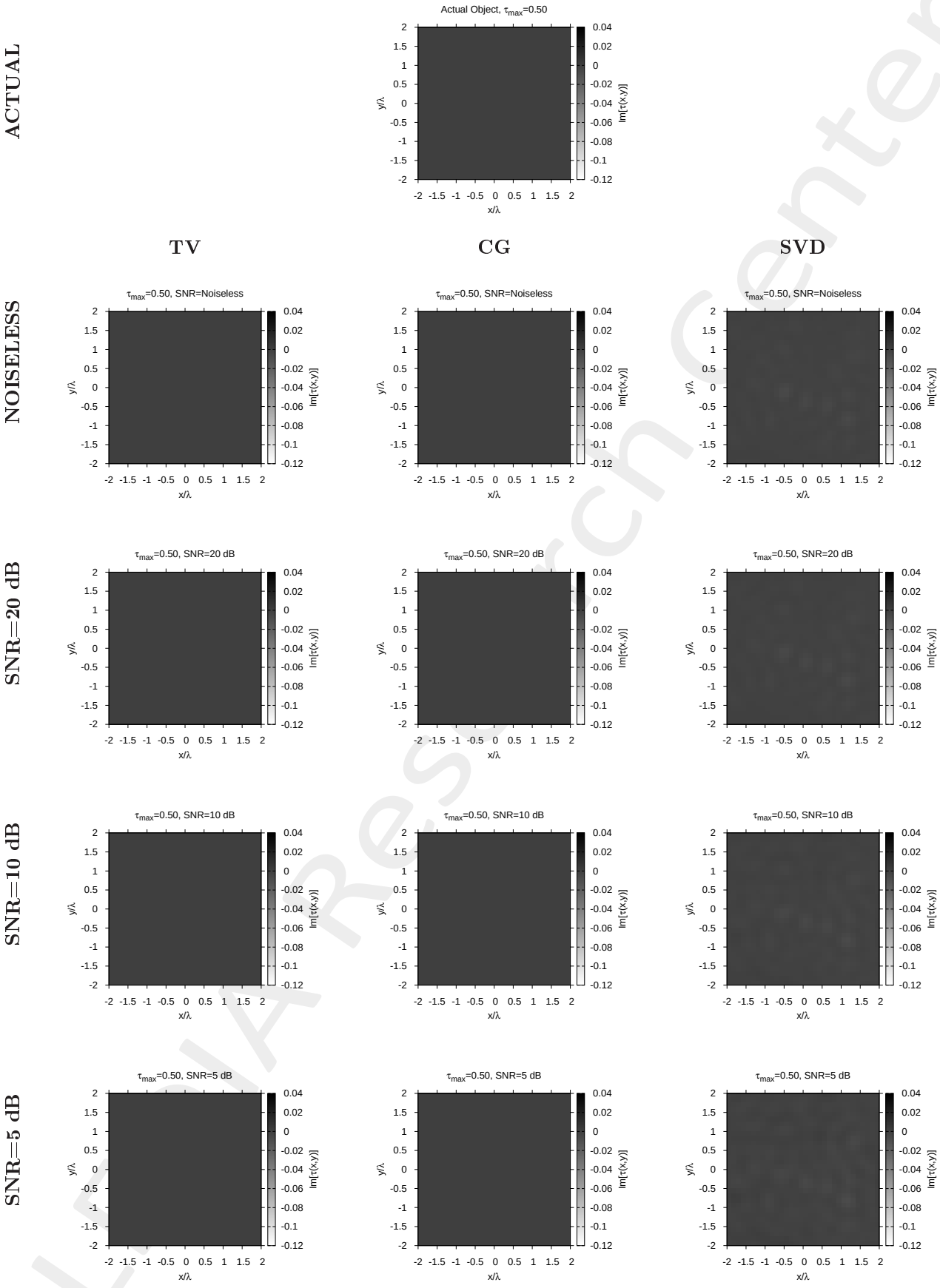

Figure 15: Actual and retrieved object considering different wavelet expansions.

SNR [dB]	**TV** [s]	**CG** [s]	**SVD** [s]	**ALPHABET** [s]
Noiseless	1.7×10^2	2.3×10^3	4.7×10^1	1.1×10^3
20	1.7×10^2	2.1×10^3	5.5×10^1	1.0×10^3
10	2.4×10^2	2.8×10^3	4.9×10^1	1.1×10^3
5	2.4×10^2	2.5×10^3	3.6×10^1	$1.0. \times 10^3$

Table 5: Timings.

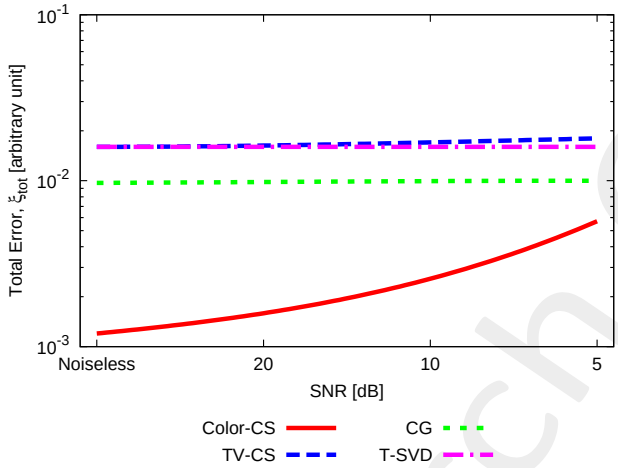

Figure 16: Comparison with SoA - Total Error vs SNR, considering $T = 99.9\%$.

More information on the topics of this document can be found in the following list of references.

References

[1] A. Massa, P. Rocca, and G. Oliveri, "Compressive sensing in electromagnetics - A review," *IEEE Antennas Propag. Mag.*, pp. 224-238, vol. 57, no. 1, Feb. 2015.

[2] A. Massa and F. Texeira, Guest-Editorial: Special Cluster on Compressive Sensing as Applied to Electromagnetics, *IEEE Antennas Wireless Propag.* Lett., vol. 14, pp. 1022-1026, 2015.

[3] G. Oliveri, N. Anselmi, and A. Massa, "Compressive sensing imaging of non-sparse 2D scatterers by a total-variation approach within the Born approximation," *IEEE Trans. Antennas Propag.*, vol. 62, no. 10, pp. 5157-5170, Oct. 2014.

[4] L. Poli, G. Oliveri, and A. Massa, "Imaging sparse metallic cylinders through a Local Shape Function Bayesian Compressive Sensing approach," *J. Opt. Soc. Am. A*, vol. 30, no. 6, pp. 1261-1272, 2013.

[5] F. Viani, L. Poli, G. Oliveri, F. Robol, and A. Massa, "Sparse scatterers imaging through approximated multitask compressive sensing strategies," *Microwave Opt. Technol. Lett.*, vol. 55, no. 7, pp. 1553-1558, Jul. 2013.

[6] M. Salucci, G. Oliveri, and A. Massa, "GPR prospecting through an inverse scattering frequency-hopping multi-focusing approach," *IEEE Trans. Geosci. Remote Sens.*, vol. 53, no. 12, pp. 6573-6592, Dec. 2015.

[7] M. Salucci, L. Poli, N. Anselmi and A. Massa, "Multifrequency particle swarm optimization for enhanced multiresolution GPR microwave imaging," *IEEE Trans. Geosci. Remote Sens.*, vol. 55, no. 3, pp. 1305-1317, Mar. 2017.

[8] M. Salucci, L. Poli, and A. Massa, "Advanced multi-frequency GPR data processing for non-linear deterministic imaging," *Signal Processing,* vol. 132, pp. 306-318, March 2017.

[9] L. Poli, G. Oliveri, P. Rocca, and A. Massa, "Bayesian compressive sensing approaches for the reconstruction of two-dimensional sparse scatterers under TE illumination," *IEEE Trans. Geosci. Remote Sens.*, vol. 51, no. 5, pp. 2920-2936, May 2013.

[10] L. Poli, G. Oliveri, and A. Massa, "Microwave imaging within the first-order Born approximation by means of the contrast-field Bayesian compressive sensing," *IEEE Trans. Antennas Propag.*, vol. 60, no. 6, pp. 2865-2879, Jun. 2012.

[11] G. Oliveri, P. Rocca, and A. Massa, "A bayesian compressive sampling-based inversion for imaging sparse scatterers," *IEEE Trans. Geosci. Remote Sens.*, vol. 49, no. 10, pp. 3993-4006, Oct. 2011.

[12] G. Oliveri, L. Poli, P. Rocca, and A. Massa, "Bayesian compressive optical imaging within the Rytov approximation," *Optics Letters*, vol. 37, no. 10, pp. 1760-1762, 2012.

[13] L. Poli, G. Oliveri, F. Viani, and A. Massa, "MT-BCS-based microwave imaging approach through minimum-norm current expansion," *IEEE Trans. Antennas Propag.*, vol. 61, no. 9, pp. 4722-4732, Sep. 2013.

[14] N. Anselmi, G. Oliveri, M. Salucci, and A. Massa, "Wavelet-based compressive imaging of sparse targets" *IEEE Trans. Antennas Propag.*, vol. 63, no. 11, pp. 4889-4900, Nov. 2015.

[15] N. Anselmi, G. Oliveri, M. A. Hannan, M. Salucci, and A. Massa, "Color compressive sensing imaging of arbitrary-shaped scatterers," *IEEE Trans. Microw. Theory Techn.*, vol. 65, no. 6, pp. 1986-1999, Jun. 2017.

[16] F. Viani, G. Oliveri, and A. Massa, "Compressive sensing pattern matching techniques for synthesizing planar sparse arrays," *IEEE Trans. Antennas Propag.*, vol. 61, no. 9, pp. 4577-4587, Sept. 2013.

[17] G. Oliveri, M. Salucci, and A. Massa, "Synthesis of modular contiguously clustered linear arrays through a sparseness-regularized solver," *IEEE Trans. Antennas Propag.*, vol. 64, no. 10, pp. 4277-4287, Oct. 2016.

[18] P. Rocca, M. A. Hannan, M. Salucci, and A. Massa, "Single-snapshot DoA estimation in array antennas with mutual coupling through a multi-scaling BCS strategy," *IEEE Trans. Antennas Propag.*, vol. 65, no. 6, pp. 3203-3213, Jun. 2017.

[19] P. Rocca, M. Benedetti, M. Donelli, D. Franceschini, and A. Massa, "Evolutionary optimization as applied to inverse problems," *Inverse Probl.*, vol. 25, pp. 1-41, Dec. 2009.

[20] P. Rocca, G. Oliveri, and A. Massa, "Differential Evolution as applied to electromagnetics," *IEEE Antennas Propag. Mag.*, vol. 53, no. 1, pp. 38-49, Feb. 2011.